Study on the adiponectin receptor agonistic di- and tripeptides by in vitro and in silico analyses

イ, ユナ

出版情報：Kyushu University, 2022, 博士（農学）, 課程博士
バージョン：
権利関係：

Study on the adiponectin receptor agonistic di- and tripeptides by *in vitro* and *in silico* analyses

Yuna Lee

Kyushu University

2022

LIST OF CONTENTS

Abbreviations

- 2-NBDG, 2-[*N*-(7-nitrobenz-2-oxa-1,3-diazol-4-yl) amino]-2-deoxy-D-glucose
- AdipoR, adiponectin receptor
- AdipoR1, adiponectin receptor 1
- AdipoR2, adiponectin receptor 2
- AdipoRon, 2-(4-benzoylphenoxy)-*N*-[1-(phenylmethyl)-4-piperidinyl]acetamide
- PKB, protein kinase B
- AMPK, adenosine monophosphate-activated protein kinase
- BSA, bovine serum albumin
- CaMKK, calcium-calmodulin-dependent protein kinase kinase
- DMEM, Dulbecco's modified Eagle's medium
- DMSO, dimethyl sulfoxide
- ESI, electrospray ionization
- FBS, fetal bovine serum
- GLUT4, glucose transporter 4
- HS, horse serum
- KRPH, Krebs-Ringer phosphate HEPES
- LC-TOF/MS, liquid chromatography-time-of-flight/mass spectrometry
- LKB1, liver kinase B1
- MD, molecular dynamics
- MM-PBSA, molecular mechanics Poisson-Boltzmann surface area
- NP-40, Nonidet P-40
- Opti-MEM, Opti-minimum essential medium
- p-AMPK, phospho (Thr172)-AMPKα1
- PBS, phosphate buffered saline
- PHT1, peptide/histidine transporter 1
- PI3K, phosphatidylinositol-3 kinase
- POPC, 1-palmitoyl-2-oleoyl-phosphatidylcholine
- PPARα, peroxisome proliferator-activated receptor α
- RIPA, radioimmunoprecipitation assay
- RMSD, root-mean-square deviation
- T1DM, type 1 diabetes mellitus
- T2DM, type 2 diabetes mellitus
- TIP3P, transferable intermolecular potential 3 point
- α-MEM, α-minimum essential medium
- ΔG_{bind}, Gibbs free energy of binding

Chapter I

General Introduction

Diabetes mellitus a global public health problem, which affected 537 million people in 2021, with projection of 783 million cases in 2045.[1] There are two major subtypes of diabetes, type 1 diabetes mellitus (T1DM) and type 2 diabetes mellitus (T2DM). Although the incidence rates of both T1DM and T2DM are growing rapidly, T2DM accounts for more than 90% of all diabetic cases.[2-3] T2DM is generally considered as a lifestyle disease since unhealthy lifestyle behaviors can contribute to its pathogenesis. The combination of excessive caloric intake and inadequate physical activity alters normal pancreatic β-cell response. Pancreatic β-cells are forced to secrete excessive insulin in the setting of fuel surplus, ultimately leading to decreased insulin sensitivity and to increased insulin resistance.[4] Thus, hyperinsulinemia is a key element of T2DM that is indicative of both β-cell dysfunction and insulin resistance. The chronic diabetes leads to serious complications such as kidney disease, vision loss, and lower-limb amputation.[5]

Adiponectin, also referred to as Acrp30,[6] AdipoQ,[7] apM1,[8] and GBP28,[9] has emerged over the past two decades as a key cytokine correlated with various disorders, including obesity, insulin resistance, and T2DM[10-11] as well as inflammation, cancer, and cardiovascular diseases.[12-14] Human adiponectin is a 244-amino acid polypeptide, which is normally produced by adipocytes. A full-length adiponectin (~30-kDa) consists of an N-terminal signal sequence, a species-specific variable region, a collagenous domain, and a C-terminal globular domain.[15] While monomeric forms are infrequently observed, adiponectin primarily circulates in the bloodstream in trimers, hexamers, and high-molecular-weight polymers, and globular forms.[16] The globular forms are produced by proteolytic cleavage of the trimer adiponectin (Fig. 1-1). The normal circulating level of adiponectin ranges from 3 to 30 μg/mL in humans, accounting for approximately 0.05% of the total plasma proteins.[17-18] Circulating adiponectin level was noticeably observed to decrease in mouse models of T2DM in which insulin resistance and hyperglycemia were induced by a high-fat diet[19] and also in T2DM patients with insulin resistance.[20] Importantly, several studies have demonstrated that supplement of adiponectin improved insulin resistance in obese and T2DM mouse models.[19,21-22] Adiponectin-overexpressing mice also exhibited improved insulin sensitivity and mitochondrial function,[23] whereas adiponectin-knockout mice are more susceptible to insulin resistance induced by a high-fat diet.[24] These findings suggest the potential of adiponectin as a therapeutic agent for metabolic diseases, especially T2DM.

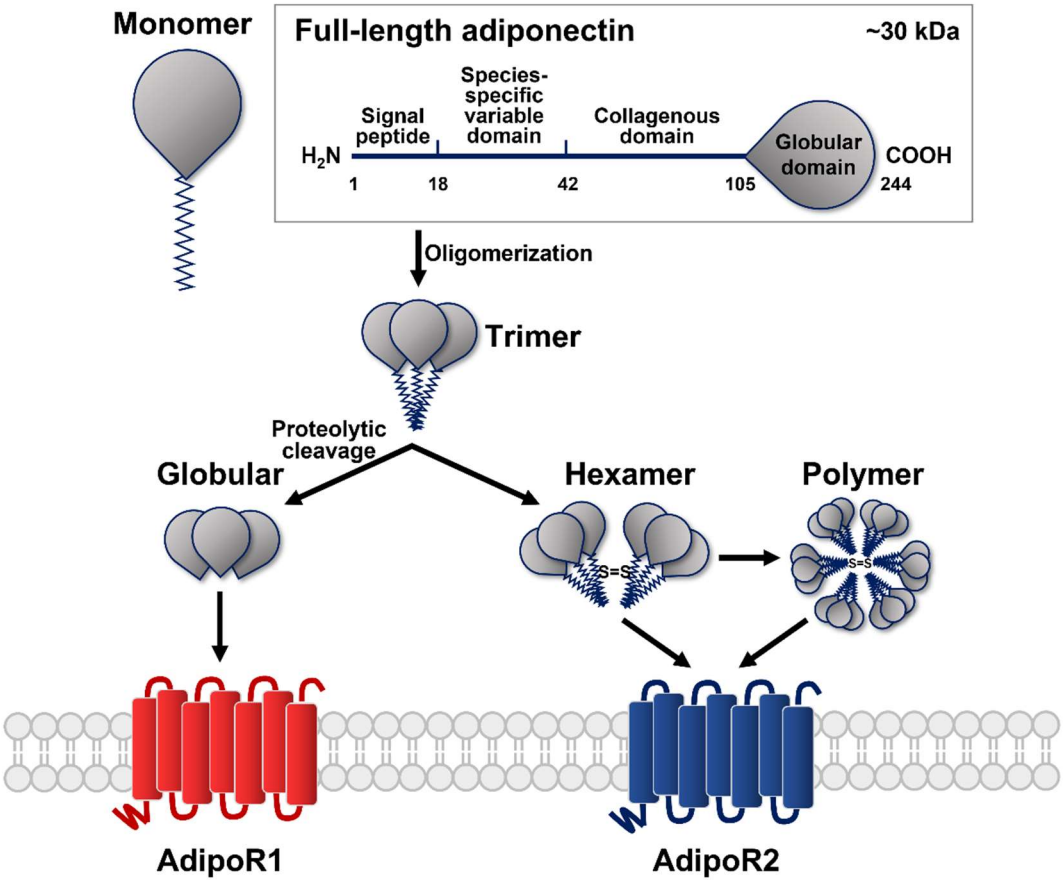

Fig. 1-1. Adiponectin structures and their receptors (AdipoR1/2).

A full-length adiponectin monomer (~30-kDa) comprises a signal sequence, a species-specific variable region, a collagenous domain, and a globular domain. Oligomerization promotes the formation of trimer, hexamer, and high-molecular-weight polymer. The globular form is a proteolytic fragment of the trimer adiponectin by proteolytic cleavage. While AdipoR1 binds to the globular form with high affinity, AdipoR2 has a moderate affinity for both globular and full-length forms.

Adiponectin is known to exert its beneficial effects, such as anti-diabetic, anti-obesity, anti-inflammatory, and cardioprotective actions, through directly binding to two distinct seven-transmembrane receptors, which are termed adiponectin receptors (AdipoR); adiponectin receptor 1 (AdipoR1) and adiponectin receptor 2 (AdipoR2).[25] The N-terminus is located intracellularly and the C-terminus is located extracellularly, which is opposite to the topology of G protein-coupled receptors.[25] It has been shown that AdipoR1 has a greater binding affinity for the globular form, while AdipoR2 has an intermediate binding affinity for both globular and full-length forms.[25-26] These two receptors are ubiquitously expressed, with the highest AdipoR1 expression in skeletal muscle and with the highest AdipoR2 expression in the liver.[25-26]

Intracellular signaling in response to binding of adiponectin to its receptors, AdipoR1/2, is mediated by an adaptor protein, APPL1 (adaptor protein with a pleckstrin homology domain, a phosphotyrosine binding domain, and a leucine zipper motif), which is known to link the AdipoR to downstream adiponectin signaling pathways.[27] Structurally, the amino acid sequences of AdipoR1/2 share 66.7% identity,[25] however, they have some functional differences in adiponectin signaling pathways. In skeletal muscle AdipoR1 mostly targets adenosine monophosphate-activated protein kinase (AMPK).[26] In the liver AdipoR2 preferentially signals to peroxisome proliferator-activated receptor α (PPARα), and it also stimulates the activation of AMPK.[26] The activation of AMPK induced by adiponectin in skeletal muscle is tightly involved in enhanced

glucose uptake, whereas the activation of PPARα by adiponectin in the liver is highly associated with regulation of lipid oxidation[26] (Fig. 1-2).

Several studies have pointed out that favorable metabolic functions induced by adiponectin in skeletal muscle and the liver was due to the activation of AMPK.[28-29] AMPK is a serine and threonine protein kinase that serves as an intracellular energy sensor in mammalian cells by controlling glucose and lipid metabolisms.[30] AMPK was shown to be critical for the regulation of lipid oxidation and insulin sensitivity by suppressing phosphorylation of acetyl-coenzyme A carboxylase in the setting of obesity and insulin resistance.[31] This results in reduction of lipid accumulation and ameliorated obesity-induced insulin resistance.[31] Adiponectin was shown to stimulate glucose transporter 4 (GLUT4) translocation from intracellular compartments to cell surface through AdipoR1-mediated AMPK-dependent pathway in skeletal muscle, resulting in increased glucose uptake.[32-33] It was also revealed that activation of AdipoR1/AMPK mediated by adiponectin can increase mitochondrial biogenesis in skeletal muscle.[34] Moreover, the lack of adiponectin action on hepatic glucose production was observed in liver-specific AMPK-deficient mice, which obviously positioned AMPK downstream from adiponectin.[35] Collectively, these observations emphasize the role of AMPK as a main downstream mediator of adiponectin signaling.

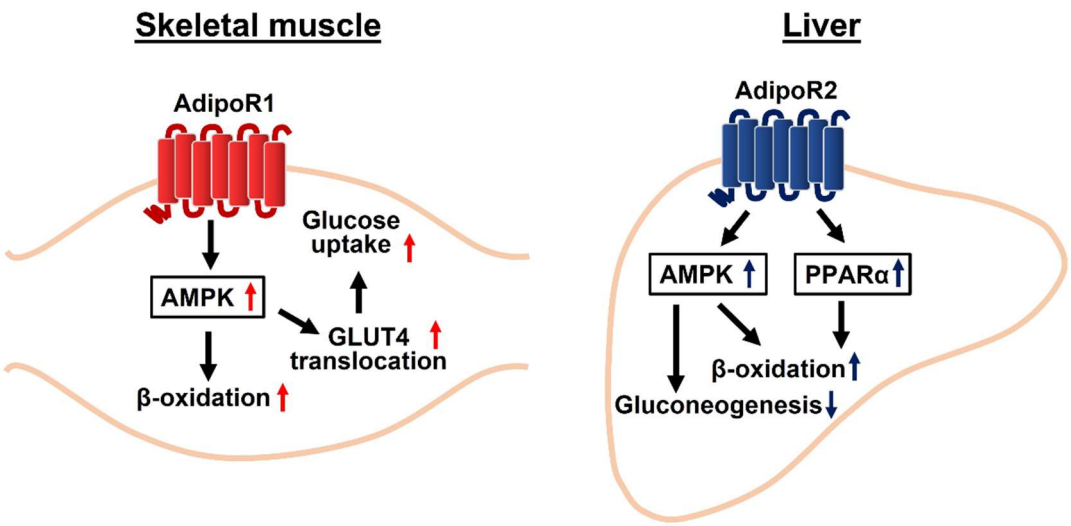

Fig. 1-2. Adiponectin signaling pathways in skeletal muscle and the liver.

Key downstream activated by adiponectin include adenosine monophosphate-activated protein kinase (AMPK) pathway and peroxisome proliferator-activated receptor α (PPARα) pathway. In skeletal muscle, adiponectin activates AMPK, thereby stimulating glucose uptake by translocation of glucose transporter 4 (GLUT4) translocation and fatty-acid oxidation. In the liver, adiponectin activates PPARα, thereby stimulating fatty-acid oxidation. It also activates AMPK, decreasing molecule associated with gluconeogenesis and increasing fatty-acid oxidation in the liver.

Although adiponectin has shown many beneficial functions including anti-diabetic effect, adiponectin-based therapeutics are currently unavailable because there are difficulties in converting this protein into a feasible drug form: (1) the heterogeneity of adiponectin structures hampers highly reproducible results *in vitro* and *in vivo*, and (2) the excessive insolubility of the C-terminal domain and larger peptide fragments thereof disrupts clinical application.[36-38] To overcome these limitations, smaller and simpler molecules that can exhibit the agonistic effect of AdipoR are required to mimic the entire protein's therapeutic effects.

So far there have been several studies on small molecules targeting AdipoR and mimicking some effects of adiponectin (Table 1-1). These AdipoR agonists can activate downstream signaling pathway to adiponectin, such as AMPK and PPARα. A decapeptide, ADP355 (Asn-Ile-Pro-Nva-Leu-Tyr-Ser-Phe-Ala-Ser) has a resembling sequence with the C-terminal domain of adiponectin and thus has a similar biological activity with globular adiponectin.[38] ADP355 targeting AdipoR1 more than AdipoR2 was shown to suppress the proliferation of cancer in several human breast cancer cells and also inhibit the growth of human breast cancer xenografts in mice.[38] ADP-1 is a highly conserved 13-residue segment peptide (Gly-Ile-Pro-Gly-His-Pro-Gly-His-Asn-Gly-Ala-Pro-Gly) from adiponectin's collagenous domain, with beneficial effects on glucose and fatty acid metabolisms.[39] It was indicated to increase glucose uptake via AdipoR1/AMPK pathway in rat skeletal muscle L6 cells and ameliorated glucose tolerance in *db/db* mice.[39] In a virtual screening study to investigate

anti-fibrotic agents, a heptapeptide, Pep70 (Pro-Gly-Leu-Tyr-Tyr-Phe-Asp) was shown to inhibit the expression of markers of fibrosis and identified as a potential AdipoR1 agonist.[40] A 15-mer oligopeptide, BHD1028 (Tyr-Tyr-Phe-Ala-Tyr-His-Pro-Asn-Ile-Pro-Gly-Leu-Tyr-Tyr-Phe) designed by *in silico* AdipoR1-ligand docking simulation was shown to activate AdipoR1-mediated signaling in mouse skeletal muscle cells.[41]

Currently, the most compelling mimic is AdipoRon, a firstly orally-active synthetic small-molecule showing AdipoR agonistic effect discovered by screening a compound library to find candidates that bind to AdipoR and greatly activate AMPK.[42] AdipoRon exerted very similar effects to those of adiponectin in muscle and the liver, such as activation of AMPK and PPARα pathways, and improved insulin resistance and glucose intolerance in mice fed with a high-fat diet, which was completely obliterated in AdipoR1/2 double-knockout mice.[42] Moreover, AdipoRon was shown to extend the shortened lifespan of T2DM model *db/db* mice in a high-fat diet.[42] Further investigations revealed its pleiotropic effects such as anti-apoptosis,[43] anti-cancer,[44] anti-depressant,[45] hepatoprotective,[46] and neuroprotective[47] properties. However, it has not yet been investigated in clinical trials, further studies on small molecule AdipoR agonists are required.

Table 1-1. Adiponectin mimetic compounds.

Compound	Target	Effect	Reference
ADP355	AdipoR1	Anti-cancer	[38]
ADP-1	AdipoR1	Anti-diabetes	[39]
Pep70	AdipoR1	Anti-fibrosis	[40]
BHD1028	AdipoR1	Anti-diabetes	[41]
AdipoRon	AdipoR1 AdipoR2	Anti-diabetes	[42]

Peptides are the collective term for short chains of amino acids, linked by peptide bonds. Bioactive peptides can be produced by enzymatic hydrolysis or food processing, from long polypeptides or proteins.[48] Depending on amino acid composition and sequence, these peptides can exert many different bioactivities, which affect cardiovascular, digestive, endocrine, immune, and nervous systems.[49-50] They must reach the target in an active form to exhibit a potential effect on human body. They need to remain active during digestion by human proteases and be transported through the intestinal wall into the blood. It is widely accepted that small peptides (di-/tripeptides) can be easily absorbed in the intestine, while it is not clear if longer oligopeptides can be absorbed and then reach the target organs.[51]

So far, many studies on small peptides (di-/tripeptides) derived from food materials involving sardine, egg, milk, and soybean have been investigated, and their potential health benefits such as anti-atherosclerosis, anti-diabetes, anti-hypertension, anti-inflammation, anti-oxidant, and memory improvement have been revealed (Table 1-2). *In vivo* absorption studies, it was revealed that intact absorbable peptides, such as anti-atherosclerotic Trp-His[52] and anti-hypertensive Val-Tyr[53], possessed high protease resistance at the apical side of the brush-border membranes in the intestine.[54-55] It was revealed that a dipeptide Tyr-Pro can be intactly transported across the blood-brain barrier, which improved memory impairment in $A\beta_{25-35}$-induced mice.[56-57] It was also reported that Pro-containing peptides, such as anti-hypertensive tripeptides Ile-Pro-Pro

and Val-Pro-Pro[58], are relatively resistant to proteolysis.[59] Moreover, these bioactive peptides have been reported to exert multiple functions. (Table 1-2).

Table 1-2. Food-derived bioactive small peptides (di- and tripeptides) and their potential health benefits.

Peptide sequence	Origin	Bioactivity	Reference
Trp-His	Sardine	Anti-atherosclerosis	[52]
		Anti-diabetes	[60]
		Anti-inflammation	[61]
Val-Tyr	Sardine	Anti-hypertension	[53]
		Anti-proliferation	[62]
Tyr-Pro	Milk Salmon Soybean	Memory improvement	[57]
		Anti-hypertension	[63]
		Anti-antioxidant	[64]
Ile-Pro-Pro Val-Pro-Pro	Milk	Anti-hypertension	[58]
		Anti-atherosclerosis	[65]
Ile-Arg-Trp	Egg	Anti-hypertension	[66]
		Anti-diabetes	[67]
		Anti-inflammation	[68]
Val-Pro-Tyr	Soybean	Anti-inflammation	[69]

Skeletal muscle is a major site of glucose disposal in the postprandial period in humans, in which more than 80% of glucose uptake occurs.[70] Glucose uptake in skeletal muscle is mediated by two distinct signaling pathways that lead to translocation of GLUT4 to the plasma membrane.[71] The first is an insulin-dependent pathway in which phosphatidylinositol-3 kinase (PI3K) is activated by insulin and then downstream protein kinase B (PKB, also known as Akt) is activated and enhances the GLUT4 translocation. The other is an insulin-independent pathway that activates AMPK to enhance the GLUT4 translocation.

The promotion of glucose uptake via AMPK activation considered a targeted approach to regulating blood glucose homeostasis. Indeed, studies of alternative-medicinal foods have provided possible improvement of impaired glucose availability by stimulating AMPK/GLUT4 pathway, independent of the insulin-dependent pathway. In rat skeletal muscle L6 cells, theasinensins, condensed catechins, promoted glucose uptake via the calcium-calmodulin-dependent protein kinase kinase (CaMKK)/AMPK/GLUT4 pathway.[72] The dipeptide Trp-His also promoted glucose uptake in L6 cells through the peptide/histidine transporter 1 (PHT1)/liver kinase B1 (LKB1)/AMPK/GLUT4 pathway.[60] Moreover, other different bioactive peptides, such as cereal proteins-derived peptides (Ile-Gln-Pro, Ile-Pro-Gln, Val-Pro-Glu, and Val-Glu-Pro)[73] and a milk casein hydrolysate-derived peptide (Ile-Pro-Pro)[74], have been revealed to promote glucose uptake via the activation of AMPK. Thus, activating insulin-independent AMPK signaling pathways by any bioactive compounds may be an effective strategy for preventing T2DM.

According to the aforementioned research background, the stimulation of AdipoR1 in skeletal muscle can be suggested as the alternative therapy of adiponectin against insulin-independent T2DM because adiponectin can promote glucose uptake in skeletal muscle through the AdipoR1-mediated AMPK/GLUT4 translocation cascade, in an insulin-independent manner. Importantly, although an orally-active synthetic small molecule showing AdipoR1/2 agonistic effect, AdipoRon was successfully developed as an adiponectin-like anti-diabetic drug, no natural AdipoR1 agonist have been reported so far. Therefore, to develop novel AdipoR1 agonist which present in natural food compounds, small peptides (in this study, di-/tripeptides) that can directly bind to and activate AdipoR1 in skeletal muscle were investigated using by *in vitro* L6 cells and *in silico* molecular dynamics (MD) simulation analyses. The present study performed with two different aspects as follows:

In **Chapter II**, among various dipeptide candidates having structural similarities with AdipoRon, a dipeptide showing great improvement of glucose uptake in rat skeletal muscle L6 cells was selected. Moreover, *in silico* MD simulation analysis was performed to clarify the binding interaction between the ligand dipeptide and AdipoR1 protein in a virtual phospholipid membrane.

In **Chapter III**, it was investigated whether tripeptides, containing dipeptide sequence determined as a great candidate in **Chapter II**, showed the AdipoR1 agonistic effect in L6 cells. The MD simulation analysis of the ligand-AdipoR1 docking complex was also performed to gain insight into the structural characterization of active tripeptides for the AdipoR1 agonistic activity.

Taken together, such small peptides can be a useful alternative anti-diabetic food compounds, with their mechanism of action involving adiponectin-like glucose uptake in skeletal muscle.

Chapter II

Adiponectin receptor agonistic action of dipeptides by *in vitro* rat skeletal muscle L6 cells and *in silico* analyses

1. Introduction

Adiponectin, an adipocyte-derived hormone,[75] directly binds to and activates two distinct receptors, adiponectin receptor 1/2 (AdipoR1/2),[25] which are mainly expressed in skeletal muscle and the liver, respectively.[26] These receptors activated by adiponectin stimulate multiple signaling pathways such as adenosine monophosphate-activated protein kinase (AMPK) and peroxisome proliferator-activated receptor α (PPARα), thereby regulating glucose and lipid metabolisms.[26] In the signaling pathway, AdipoR1 seems to be more tightly associated with the activation of AMPK pathway, while AdipoR2 seems to be linked to the activation of PPARα pathway.[26] Thus far, it has been reported that the intracellular signaling axis of adiponectin hormone towards glucose uptake

in skeletal muscle mainly involves AdipoR1-mediated AMPK-dependent glucose transporter 4 (GLUT4) translocation pathway.[28,32-33] Therefore, stimulating AdipoR1 in skeletal muscle may help to improve insulin resistance in type 2 diabetes mellitus (T2DM) in an insulin-independent manner.

AdipoRon is an orally-active synthetic analogue that mimics the actions of adiponectin by both stimulating AdipoR1/2.[42] It was demonstrated that impaired glucose tolerance and insulin resistance in *db/db* mice fed with a high-fat diet was ameliorated by the oral administration of AdipoRon (50 mg/kg).[42] Recent reports also claimed *in vivo* biological effectiveness of AdipoRon in restoring renal AdipoR1/2 expression[76] and improved vascular dysfunction in *db/db* mice.[77] Although these findings led to investigation of a strategy for regulation or prevention of T2DM with obesity-related glucose tolerance by adiponectin-like food compounds, no alternative-medicinal food studies regarding an adiponectin-like natural agonist have been reported so far.

The aim of this **Chapter II** was to discover AdipoR1 agonistic dipeptides, since the structural features of AdipoRon, with characteristic 1-benzyl-4-substituted 6-membered cyclic amine moieties and aromatic rings linked with amide bonds (Fig. 2-1), can be mimicked by a peptide skeleton bearing aromatic rings and peptide bonds. In a previous report, 15-mer oligopeptides (BHD1028) designed by *in silico* AdipoR1 protein-ligand docking simulation of the crystal structure were confirmed to activate AdipoR1-mediated signaling pathway in mouse skeletal muscle cells.[41] Although the report revealed the possible

development of a peptide-derived AdipoR1 agonist, the present *in vitro* study on AdipoR1 agonistic dipeptides in rat skeletal muscle L6 cells is novel, and distinct from the report by Kim *et al*.[41] *In vivo* peptide absorption studies,[53-54] dipeptides are preferably absorbed into the blood system in intact forms, while few evidence of intact absorption of longer oligopeptides, including 15-mer oligopeptides, has been reported. The advantage of dipeptides may thus allow the development of "orally-active" functional peptides exerting AdipoR1-mediated prevention of T2DM. Another novelty of this study lies in the *in silico* molecular dynamics (MD) simulation using the CHARMM-GUI, in which membrane-embedded AdipoR1 is virtually anchored in the phospholipid membrane, and the molecular interaction of AdipoR1 agonist dipeptides with the AdipoR1 protein could be validated in virtual physiological environments.

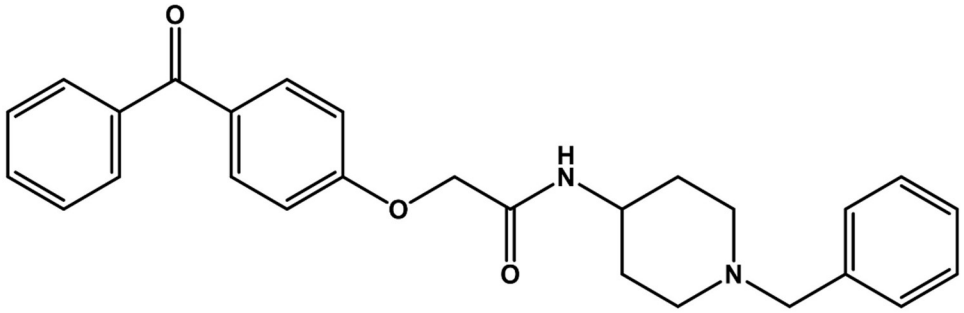

Fig. 2-1. Chemical structure of AdipoRon (2-(4-benzoylphenoxy)-*N*-[1-(phenylmethyl)-4-piperidinyl]acetamide).

2. Materials and Methods

2.1. Materials

AdipoRon (>98% pure) was acquired from Cayman Chemical (Ann Arbor, MI, USA). Insulin and dimethyl sulfoxide (DMSO, 99.9%) were obtained from Sigma-Aldrich (St. Louis, MO, USA). Dulbecco's modified Eagle's medium (DMEM), fetal bovine serum (FBS), horse serum (HS), and Opti-minimum essential medium (Opti-MEM) were purchased from Gibco (Grand Island, NY, USA). α-minimum essential medium (α-MEM) was purchased from FUJIFILM Wako Pure Chemical Co. (Osaka, Japan). 2-[*N*-(7-nitrobenz-2-oxa-1,3-diazol-4-yl) amino]-2-deoxy-D-glucose (2-NBDG) was obtained from Invitrogen (Carlsbad, CA, USA). Compound C (an AMPK inhibitor) was purchased from Merch Millipore (Darmstadt, Germany). The following dipeptides were purchased from Kokusan Chemical Co. (Tokyo, Japan): Tyr-Pro (YP), Pro-Tyr (PY), Tyr-His (YH), His-Tyr (HY), Tyr-Trp (YW), Trp-Tyr (WY), Phe-Pro (FP), Pro-Phe (PF), Phe-His (FH), His-Phe (HF), Phe-Trp (FW), Trp-Phe (WF), Ile-Pro (IP), Trp-Pro (WP), His-Pro (HP), and Trp-His (WH). Other chemicals were of analytical grade and used without further purification.

2.2. Cell culture

Rat skeletal muscle L6 myoblasts were obtained from the Japanese Collection of Research Bioresources (JCRB 9081; JCRB Cell Bank, Osaka, Japan). The L6 myoblasts were grown in DMEM supplemented with 10% FBS, 1% non-essential amino acids, 2 mM L-glutamine, 100 U/mL penicillin, 100 μg/mL streptomycin, 1.7 μM insulin, and 44 mM $NaHCO_3$ at 37°C in a humidified atmosphere with 5% CO_2. When the myoblasts reached 80% confluence, they were transferred to DMEM containing 2% HS for differentiation. The medium was refreshed every other day to obtain mature L6 myotubes for at least 5 days. Prior to performing each experiment, the differentiated L6 myotubes were serum-starved in α-MEM supplemented with 0.2% bovine serum albumin (BSA) for 18 h.

2.3. Glucose uptake assay

Glucose uptake into L6 myotubes was evaluated using a 2-NBDG fluorescence assay[78] as previously described method[72] with slight modifications. L6 myoblasts were seeded at 1,500 cells/well in a type I collagen-coated 96-well black microplate (NCO3904; Corning Inc., Corning, NY, USA) and grown until they formed mature L6 myotubes. After serum starvation, the L6 myotubes were rinsed twice with warm Krebs–Ringer phosphate HEPES (KRPH) buffer, consisting of 118 mM NaCl, 5 mM KCl, 1.2 mM KH_2PO_4, 1.3 mM $CaCl_2$, 1.2 mM $MgSO_4$, and 30 mM HEPES (pH 7.4). The myotubes were then incubated with 100 μL of the respective peptide sample (0.1–10 μM, 0.5–2 h) in 0.1% DMSO/KRPH buffer. An AMPK inhibition experiment was conducted by addition of 20 μM Compound C to the peptide sample. AdipoRon (0.1 μM, 0.5 h) and insulin (0.1 μM, 0.5 h) were used as a positive control to validate the 2-NBDG uptake experiments. Next, 100 μL of 100 μM 2-NBDG solution dissolved in KRPH buffer was added to each well and incubated for 1 h. At the end of the treatment, the myotubes were rinsed with thrice with ice-cold KRPH buffer to terminate the reaction. The fluorescence intensity of 2-NBDG was measured at excitation and emission wavelengths of 465 and 540 nm, respectively, using a Flex Station II scanning fluorometer (Molecular Devices, Sunnyvale, CA, USA). The fluorescent intensity of 2-NBDG uptake in the samples was assessed relative percentage (%) to the fluorescence intensity of the control (L6 myotubes incubated with 2-NBDG alone).

2.4. Knockdown of AdipoR1 using siRNA transfection

L6 cells were transfected with either AdipoR1 siRNA (sc-156024, Lot: G1321; Santa Cruz Biotechnology, Santa Cruz, CA, USA) or negative control siRNA (sc-37007, Lot: 11418; Santa Cruz Biotechnology) according to the manufacturer's protocol with slight modifications. Briefly, the cells were seeded at 1,500 cells/well in a 96-well microplate (for 2-NBDG uptake assay) or 1×10^5 cells/well in a 6-well microplate (for immunodetection assay) and then transfected with 20 nM siRNA dissolved in Opti-MEM, using a Hiperfect transfection reagent (QIAGEN, Hilden, Germany). After 6 h, the medium was replaced with 2% HS/DMEM medium. The cells were differentiated for an additional 5 days and then re-transfected using the same method. Subsequently, the transfected cells were used for either 2-NBDG uptake assay or immunodetection assay. Non-transfected cells were used as a control.

To detect the level of AdipoR1, the transfected cells were rinsed twice with ice-cold phosphate buffered saline (PBS), collected with a cell scraper in a radioimmunoprecipitation assay (RIPA) buffer (50 mM Tris-HCl, pH 8.0, 150 mM NaCl, 0.5% sodium deoxycholate, 0.1% sodium dodecyl sulfate, and 1% Nonidet P-40 (NP-40)) containing a protease inhibitor cocktail (Nacalai Tesque, Kyoto, Japan) and a phosphatase inhibitor tablet (PhosSTOP, Roche, Basel, Switzerland), and homogenized with a polytron homogenizer (Kinematica AG, Luzern, Switzerland) at 20,000 rpm for 30 s at 4°C. After centrifugation (20,000 × *g*, 20 min, 4°C), the supernatant was gathered as the cell lysate.

2.5. Phosphorylation of AMPK

L6 myoblasts were seeded at 1×10^5 cells/well in a 6-well microplate and then the differentiated L6 myotubes were treated with YP (1 μM, 1 h) or AdipoRon (0.1 μM, 0.5 h). After being treated with the samples, the myotubes were rinsed twice with ice-cold PBS, collected with a cell scraper in RIPA buffer containing protease and phosphatase inhibitors, and then centrifuged (20,000 × *g*, 20 min, 4°C) to acquire the supernatant as the cell lysate.

2.6. GLUT4 translocation assay

L6 myoblasts were seeded at 4×10^5 cells/well in a 6-well microplate and then the differentiated L6 myotubes were treated with either YP (1 μM, 1 h) or AdipoRon (0.1 μM, 0.5 h), in the presence or absence of 20 μM Compound C. To detect the level of GLUT4 translocation in the cells, the plasma membrane was extracted according to the previous method[79] with several modifications. After rinsing twice with ice-cold PBS, the sample-treated cells were suspended in ice-cold lysis buffer (50 mM Tris-HCl, 0.5 mM dithiothreitol, pH 8.0) containing 0.1% NP-40 and protease and phosphatase inhibitors and homogenized. The homogenate was then centrifuged (1,000 × *g*, 10 min, 4°C) to acquire a pellet. The pellet was suspended in the lysis buffer with the same inhibitors, kept on ice for 10 min, and then centrifuged (1,000 × *g*, 10 min, 4°C). The resulting pellet was re-suspended in the lysis buffer containing 1% NP-40 and the same inhibitors on ice for 1 h with intermittent agitation. After centrifugation (20,000 × *g*, 20 min, 4°C), the supernatant was gathered as the plasma membrane.

To extract the whole cell lysate, part of the homogenate prepared as described above was added with an equal volume of 2 × RIPA buffer with the same inhibitors and kept on ice for 1 h with intermittent agitation. After centrifugation (20,000 × *g*, 20 min, 4°C), the supernatant was gathered as the cell lysate.

2.7. The WES analysis

A capillary electrophoretic-based immunoassay was conducted to measure target protein levels by a WES instrument (ProteinSimple Co., San Jose, CA, USA), according to the manufacturer's protocol; a 12–230 kDa separation module (8 × 25 mm capillary cartridge) was used. Briefly, the samples were mixed with 5× fluorescent denaturing master mix and 0.1× sample diluent buffer to obtain 0.5 μg/μL loading protein concentration (except for GLUT4 detection: 0.8 μg/μL of cell lysate, 2.0 μg/μL of plasma membrane). The samples were then treated for 5 min at 95°C (except for GLUT4 detection: 20 min, 37°C). The primary antibodies used were as follows: AMPK (1:100 dilution, anti-rabbit, 07-350, Lot: 2922422; Merch Millipore), p-AMPK (1:100 dilution, anti-rabbit, 07-681, Lot: 2901522; Merch Millipore), AdipoR1 (1:50 dilution, anti-rabbit, ab126611, Lot: GR277137-17; Abcam, Cambridge, UK), and GLUT4 (1:10 dilution, anti-mouse, 2213S, Lot: 7; Cell Signaling Technology, Danvers, MA, USA). The samples, biotin-labeled protein ladder, blocking reagent, primary antibodies, horseradish peroxidase-conjugated secondary antibodies, and chemiluminescent substrate were dispensed into the supplied microplate. A total protein assay was conducted to normalize the target protein signal using a pentafluorophenyl ester-biotin labeling reagent. Following plate loading, electrophoresis and immunodetection were conducted in a fully automated capillary system. The data were displayed as a virtual blot-like image and an electropherogram based on the molecular weight by a Compass software

(ProteinSimple Co.). Protein expression of AdipoR1 and GLUT4 was normalized using the electropherogram peak area of total protein applied in each lane, and the date were expressed as the ratios against control.

2.8. Structure optimization of ligands and AdipoR1 protein

The initial structure of AdipoRon (Compound ID 16307093) was obtained from PubChem, and its geometry was optimized at the B3LYP/6–31G(d) level using a Gaussian ver. 16A. 03. The antechamber implemented in an AMBER ver. 18 was used to generate the restrained electrostatic potential charges of the ligand. YP was constructed using a Chimera ver. 1.14, and it was mutated to create other ligands (PY and WP) using a CHARMM-GUI-mutation.[80]

The crystal structure of human AdipoR1 protein (PDB ID 3WXV) from the RCSB Protein Data Bank was utilized as a template for ligand docking. AdipoR1 structure was modified to create an appropriate protein model for docking study: (1) Unnecessary parts (nanobodies) were removed from the initial structure using a PyMOL ver. 2.3.4. (2) Missing amino acid residues (Pro^{159}, Asn^{160}, Gly^{298}, and Gln^{299}) in the template were inserted using a MODELLER ver. 9.23. The input alignment for modeling was acquired using a ClustalW ver. 2.1 based on the human AdipoR1 sequence retrieved from UniProt Knowledgebase (UniProtKB ID Q96A54). (3) a missing zinc ion was added into the MODELLER-reconstructed AdipoR1 protein to obtain the complete structure (Fig. 2-2).

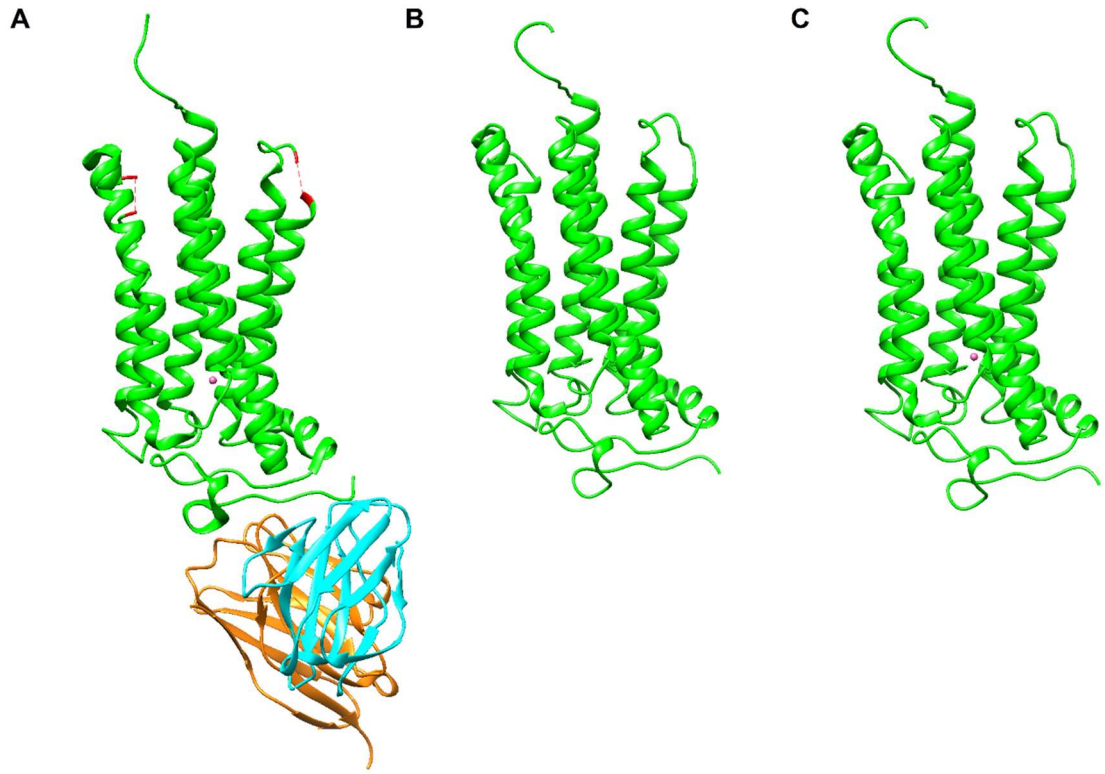

Fig. 2-2. The three-dimensional structure of AdipoR1.

(A) Missing amino acid residues in the initial structure of AdipoR1 (PDB ID 3WXV) were indicated by red regions. (B) The AdipoR1 structure was reconstructed by repairing the missing residues. (C) To obtain the complete structure, a missing zinc ion (purple sphere) was added into the reconstructed AdipoR1 structure.

2.9. Molecular docking and molecular dynamics (MD) simulation

Molecular docking of the ligand in the AdipoR1 protein was conducted using an AutoDock Tools ver. 1.5.6. Ligand-binding sites in AdipoR1 were determined based on the two presumed binding pockets (sites 1/2) of adiponectin to AdipoR1 as described in previous study.[41] The grid-box parameters used in this study were listed in Table 2-1.

MD simulation was performed using the Fujitsu PRIMERGY CX2570 M4 supercomputer of the Research Institute for Information Technology of Kyushu University. To conduct MD simulation of ligand with AdipoR1 protein anchored in a virtual 1-palmitoyl-2-oleoyl-phosphatidylcholine (POPC) membrane, the POPC bilayer was constructed by a CHARMM-GUI membrane builder.[80] The POPC lipid system was solvated using a transferable intermolecular potential with three points (TIP3P) for molecules, and then 0.15 M NaCl was added to mimic the physiological condition.[81] The AMBER ff14SB[82], lipid14[83], and the general AMBER force field 2[84] were used to construct the dipeptides and AdipoR1, POPC, and AdipoRon, respectively. The MD simulation of the virtual system was conducted using an AMBER.[85] Energy minimization and equilibration of the dipeptide-AdipoR1 complex in the POPC membrane were implemented at 310 K and a pressure of 1.0 atm for 200 ns. The protein backbone root-mean-square deviation (RMSD) of the complex in the POPC was used to assess the stability of the virtual system in this study.

Table 2-1. Grid-box parameters for docking.

Grid-box parameters		Site 1	Site 2
Center (Å)	*x*	21.654	21.959
	y	64.273	59.570
	z	3.079	-7.978
Size (Å)	*x*	14	10
	y	28	22
	z	8	8

After the MD simulation, to assess the binding affinities between the dipeptide and AdipoR1 in the POPC system, the Gibbs free energy of binding (ΔG_{bind}) was estimated during the last 20 ns of the simulation (180–200 ns, 200 frames), using the molecular mechanics Poisson–Boltzmann surface area (MM-PBSA) method.[86] The equation used was as follow:

$$\boldsymbol{\Delta G_{bind} = G_{complex} - (G_{ligand} + G_{protein})}$$

Where $G_{complex}$ represents the total free energy of the ligand-AdipoR1-POPC complex in the water system, and G_{ligand} and $G_{protein}$ represent the total free energies of the ligand and AdipoR1 alone in the water system, respectively. Only the enthalpic components were considered in the computational estimation.

Intermolecular interactions between the ligand and AdipoR1 were observed, and hydrogen bonds, hydrophobic, and π–π electron interactions in the complex were visualized using a Proteins*Plus* server. The hydrogen bond distances were calculated during 180–200 ns simulation using a Chimera.

2.10. LC-TOF/MS analysis

The dipeptides in medium were assessed using a liquid chromatography-time-of-flight/mass spectrometry (LC-TOF/MS). The medium was passed through a Merck Millipore 0.2 μm-polytetrafluoroethylene membrane filter, and 20 μL of the filtrate was injected into a LC-TOF/MS. The chromatographic separation was carried out by an Agilent 1200 series HPLC system (Agilent Technologies, Waldbronn, Germany) that was equipped with a Cosmosil $5C_{18}$-MS-II column (2.0 × 150 mm, Nacalai Tesque) and eluted with a linear gradient of water containing 0.1% formic acid to methanol containing 0.1% formic acid (20 min) at flow rate of 0.2 mL/min at 40°C. TOF/MS analysis was conducted using a Bruker micrOTOF-II MS equipment (Bruker Daltonics, Bremen, Germany) in electrospray ionization (ESI)-positive ion mode ($[M + H]^+$ for YP and PY: 279.1353 *m/z*). The MS conditions were set as follows: drying N_2 gas, 8.0 L/min; drying temperature, 200°C; nebulizer pressure, 1.6 bar; capillary voltage, 4,500 V; mass range, 100–1,000 *m/z*. A calibration solution (10 mM sodium formate in 50% acetonitrile) was injected at the beginning of each run, and all spectra were calibrated internally. Data acquisition and analysis were performed using a Bruker Data Analysis ver. 3.2.

2.11. Statistical analysis

Results are presented as mean ± standard error of the mean (SEM). Statistical differences within groups were assessed by one-way analysis of variance (ANOVA), followed by Dunnett's *t*-test for post hoc analysis. Statistical differences between two groups were evaluated using unpaired two-tailed Student's *t*-test. A $p < 0.05$ was regarded as statistically significant. All analyses were performed using GraphPad Prism ver. 5.0 (La Jolla, CA, USA).

3. Results and Discussion

3.1. Screening for dipeptides that promote 2-NBDG uptake in L6 myotubes

An AdipoR agonist, AdipoRon, was designed to exert adiponectin-like actions by its characteristic 1-benzyl 4-substituted 6-membered cyclic amine moiety and aromatic rings linked with amide bond[42] (Fig. 2-1). Referring to the required structural information of AdipoRon for AdipoR1 binding, twelve aromatic dipeptides were firstly targeted (YP, PY, YH, HY, YW, WY, FP, PF, FH, HF, FW, and WF). The dipeptide candidates were subjected to glucose (or 2-NBDG) uptake experiments in rat skeletal muscle L6 myotubes at a concentration of 10 μM. Among them, two dipeptides of YP (150 ± 14%, $p < 0.05$) and FP (133 ± 14%, $p = 0.08$) were found as candidates for promoting 2-NBDG uptake in L6 myotubes, similar to insulin (0.1 μM, 166 ± 8%) and AdipoRon (0.1 μM, 162 ± 12%) under the present experimental conditions. In contrast, PY and PF with reversed sequences of the above two active peptides failed to promote the uptake (Fig. 2-3). This observation led to a consideration of the importance of peptide sequence and imino group from Pro positioned at the C-terminus in exerting glucose promotion effect in L6 myotubes.

Hence, four C-terminal Pro-containing dipeptides (IP, WP, HP, and YP) were newly targeted for further screening of 2-NBDG-promoting dipeptides in L6 myotubes. As shown in Fig. 2-4, no significant promoting effect of the Pro-dipeptides, except for YP ($p < 0.05$), was observed, suggesting that aromatic amino acids at the N-terminus of Pro-dipeptides are not a determining factor for

this effect. No increase in 2-NBDG uptake by a mixture of Tyr and Pro (Fig. 2-4) strongly indicates the importance of the peptide structure of YP for glucose promotion.

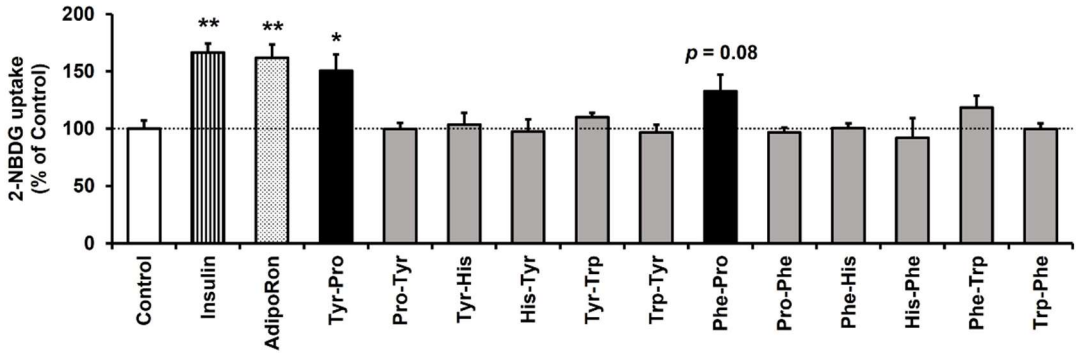

Fig. 2-3. Screening of twelve dipeptides promoting glucose uptake in L6 myotubes.

2-NBDG uptake experiment of twelve dipeptides (YP, PY, YH, HY, YW, WY, FP, PF, FH, HF, FW, and WF) was performed at 10 μM for 0.5 h in L6 myotubes. 0.1 μM insulin and 0.1 μM AdipoRon were used as a positive control. Results are presented as mean ± SEM (n = 4). Statistical differences were assessed by unpaired two-tailed Student's t-test. *$p < 0.05$, **$p < 0.01$ *vs*. Control.

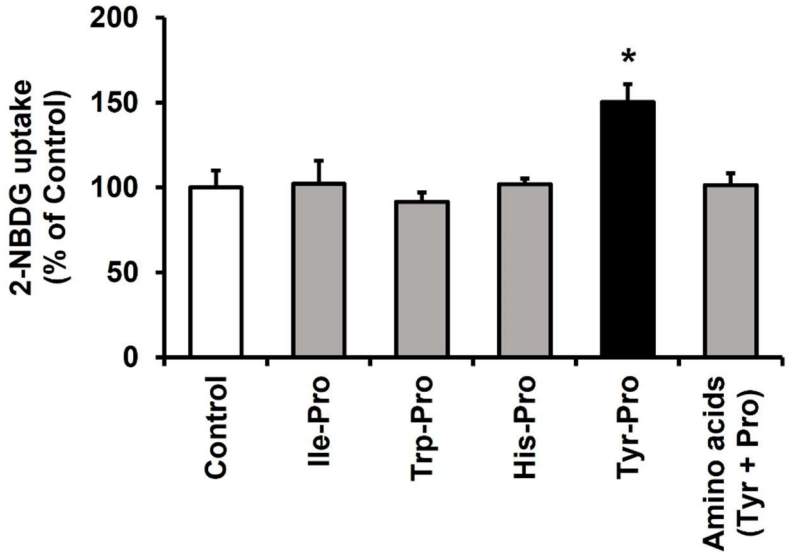

Fig. 2-4. Screening of four dipeptides promoting glucose uptake in L6 myotubes.

2-NBDG uptake experiment of four dipeptides containing Pro at the C-terminus (IP, WP, HP, and YP) and a mixture of Tyr and Pro (Tyr + Pro) was performed at 10 μM for 0.5 h in L6 myotubes. Results are presented as mean ± SEM (n = 4). Statistical differences were assessed by unpaired two-tailed Student's t-test. *p < 0.05 *vs*. Control.

3.2. Promotion of glucose uptake by Tyr-Pro (YP) in L6 myotubes

The potential of YP on 2-NBDG uptake was investigated as a function of concentration (0.1, 1, or 10 μM) or incubation time (0.5, 1, or 2 h). As shown in Fig. 2-5, a significant promoting response of YP ($p < 0.05$) was acquired at a concentration of more than 1 μM when L6 myotubes were treated for 0.5 h. Meanwhile, FP, which tended to promote the uptake at 10 μM (Fig. 2-3), failed to promote uptake at lower concentration (Fig. 2-5), suggesting that the dipeptide was categorized as a weak glucose promoter. The promoting effect of YP was time-dependent, achieving the maximal promoting effect at 1 h (174 ± 23%) (Fig. 2-6). Thus, further experiments of active YP were conducted at 1 μM concentration for 1 h.

Among the reported natural compounds with glucose-promoting effects, YP present in soybean hydrolysate at 470 μg/g-hydrolysate[56] may be categorized as a potent promotor for glucose uptake, since other natural compounds, such as 6-*O*-caffeoylsophorose (179 ± 18%, 100 μM, 1 h),[87] theasinensins (ca. 200%, 50 μM, 1 h),[72] rosmarinic acid (186 ± 4%, 5 μM, 4 h),[88] and naringenin (193 ± 24%, 75 μM, 2 h),[89] showed weaker glucose uptake potency in L6 myotubes than that of YP (174 ± 23%, 1 μM, 1 h).

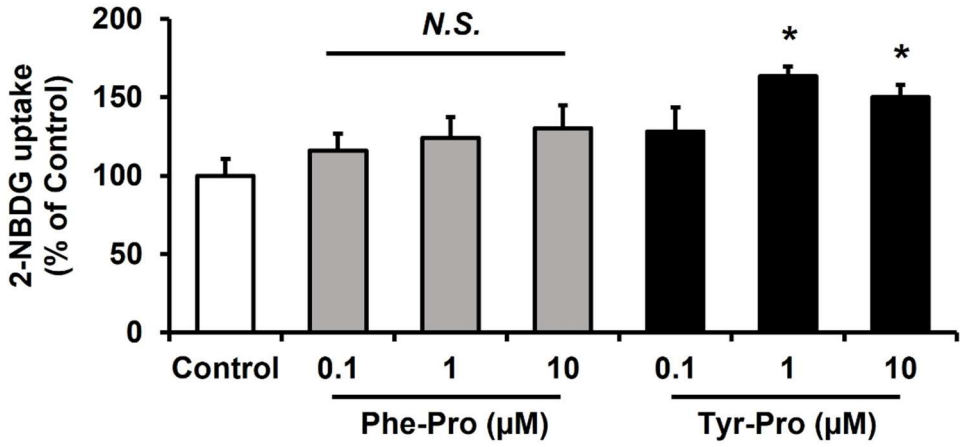

Fig. 2-5. Concentration-effect of YP on glucose uptake in L6 myotubes.

L6 myotubes were incubated with 0.1, 1, or 10 μM dipeptides for 0.5 h to evaluate the effect of FP or YP concentrations on 2-NBDG uptake. Results are presented as mean ± SEM (n = 4). Statistical differences were assessed by Dunnett's t-test. *$p < 0.05$ *vs*. Control; *N.S.*, no significant difference at $p > 0.05$.

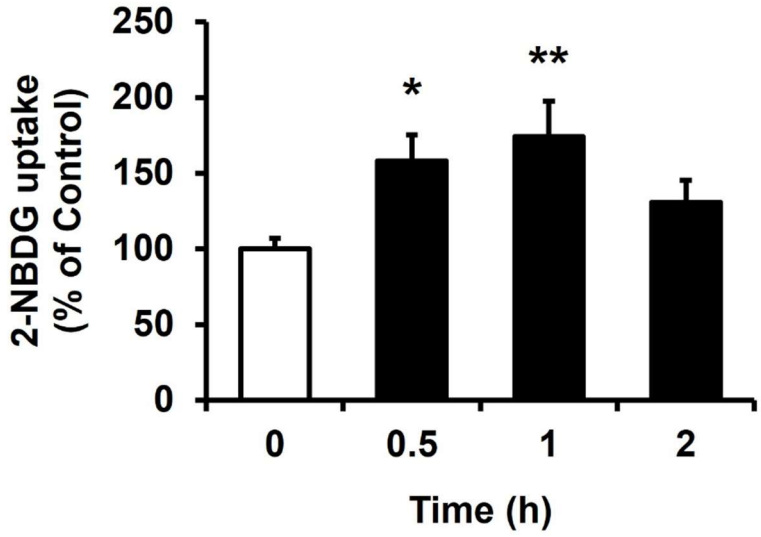

Fig. 2-6. Time-effect of YP on glucose uptake by in L6 myotubes.

L6 myotubes were incubated for 0.5, 1, or 2 h to evaluate the effect of incubation time with 1 μM YP on 2-NBDG uptake. Results are presented as mean ± SEM (n = 4). Statistical differences were assessed by Dunnett's t-test. *$p < 0.05$, **$p < 0.01$ *vs*. Control.

3.3. Involvement of AdipoR1 in YP-induced glucose uptake in L6 myotubes

The involvement of AdipoR1 in promoting 2-NBDG uptake by AdipoRon-mimicking YP was examined in AdipoR1-knockdown L6 myotubes. The AdipoR1-knockdown in L6 myotubes by AdipoR1-specific siRNA transfection (Fig. 2-7) resulted in a significant disappearance of YP-induced promotion of 2-NBDG uptake (Fig. 2-8). A similar reduction in uptake in the knockdown cells was also observed for the AdipoR1 agonist AdipoRon (Fig. 2-8), indicating that the promotion by both AdipoRon and YP was mediated by AdipoR1 in L6 myotubes. The observed YP sequence-specific promotion via AdipoR1 recognition was also validated by the lack of change in the glucose uptake of WH,[60] a peptide/histidine transporter 1 (PHT1) (but not AdipoR1)-mediated promoter of glucose uptake in AdipoR1-knocked down L6 myotubes.

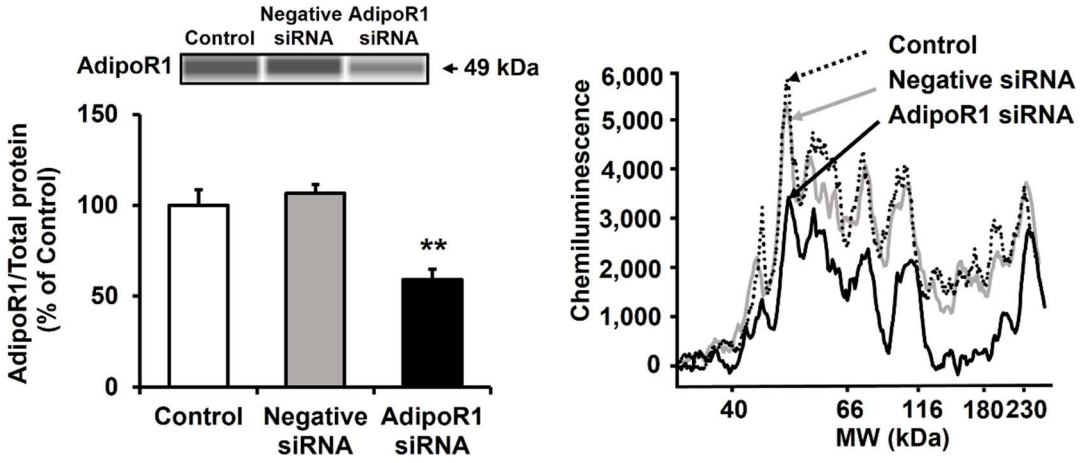

Fig. 2-7. AdipoR1-knockdown in L6 myotubes by siRNA transfection.

The level of AdipoR1 was measured by the WES analysis in AdipoR1-knockdown L6 myotubes by AdipoR1-specific siRNA transfection. Results are displayed as virtual blot-like images and electropherograms. Results are presented as mean ± SEM (n = 4–5). Statistical differences were assessed by Dunnett's t-test. $^{**}p < 0.01$ *vs*. Control.

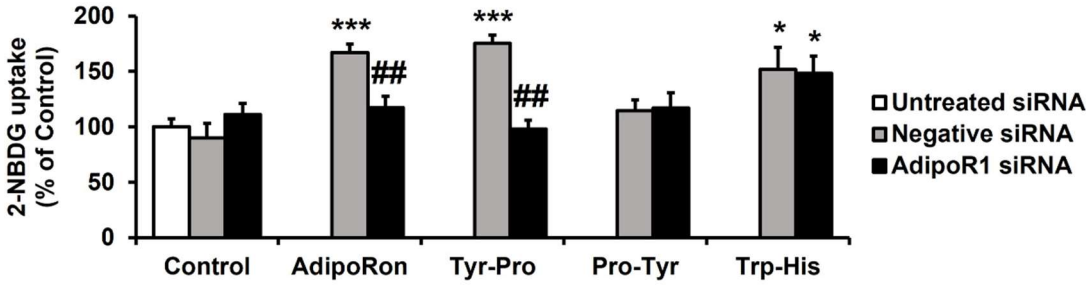

Fig. 2-8. Involvement of the AdipoR1 in promoting glucose uptake by YP in L6 myotubes.

The knockdown L6 myotubes were incubated with AdipoRon (0.1 μM, 0.5 h), YP (1 μM, 1 h), PY (1 μM, 1 h), or WH (10 μM, 1 h) to evaluate the effect of AdipoR1-knockdown in L6 myotubes on the promotion of 2-NBDG uptake by dipeptides. Results are presented as mean ± SEM (n = 4–5). Statistical differences were assessed by Dunnett's t-test. $^{**}p < 0.01$, $^{***}p < 0.001$ *vs*. Control. Statistical differences between negative and AdipoR1 siRNA groups were assessed by unpaired two-tailed Student's t-test. $^{\#\#}p < 0.01$.

3.4. Effect of YP on AMPK-mediated GLUT4 translocation in L6 myotubes

To clarify the mechanism of the promotion of glucose uptake by YP, the translocation of GLUT4 in L6 myotubes was investigated. As shown in Fig. 2-9, the AMPK signaling inhibition by Compound C abolished ($p < 0.05$) the promotion of 2-NBDG uptake by YP, similar to AdipoRon. AMPK activation in L6 myotubes treated with YP and AdipoRon was also confirmed by an increase in the phosphorylation level of AMPK (Fig. 2-10). As shown in Fig. 2-11, GLUT4 expression in the plasma membrane of L6 myotubes was promoted by YP, similar to AdipoRon, indicating that YP may stimulate the GLUT4 translocation via the activation of AdipoR1/AMPK signaling.

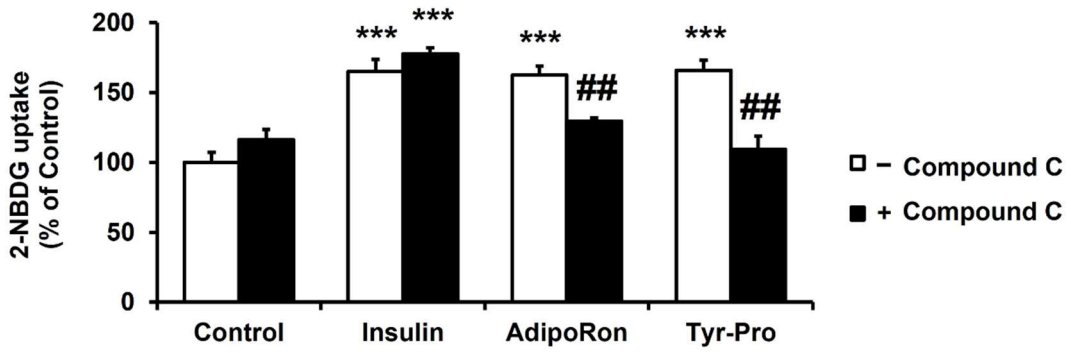

Fig. 2-9. Involvement of AMPK activation in promoting 2-NBDG uptake by YP in L6 myotubes.

L6 myotubes were incubated with insulin (0.1 μM, 0.5 h), AdipoRon (0.1 μM, 0.5 h), or YP (1 μM, 1 h) in the presence or absence of Compound C (20 μM; an AMPK inhibitor) to evaluate the effect of Compound C in promoting 2-NBDG uptake by YP in L6 myotubes. Results are presented as mean ± SEM (n = 3–5). Statistical differences were assessed by Dunnett's t-test. $^{***}p < 0.001$ *vs*. Control. Statistical differences between two groups in the presence or absence of Compound C were assessed by unpaired two-tailed Student's t-test. $^{\#\#}p < 0.01$.

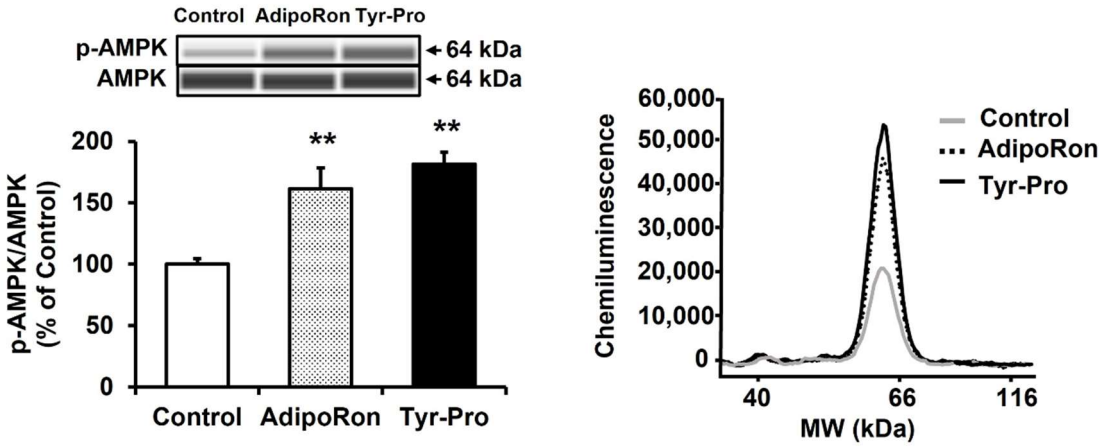

Fig. 2-10. Effect of YP on AMPK phosphorylation in L6 myotubes.

The levels of AMPK and p-AMPK in L6 myotubes treated with AdipoRon (0.1 μM, 0.5 h) or YP (1 μM, 1 h) were measured by the WES analysis to evaluate the effect of YP on AMPK phosphorylation. Results are displayed as virtual blot-like images and electropherograms. Results are presented as mean ± SEM (n = 3–5). Statistical differences were assessed by Dunnett's t-test. $^{**}p < 0.001$ *vs*. Control.

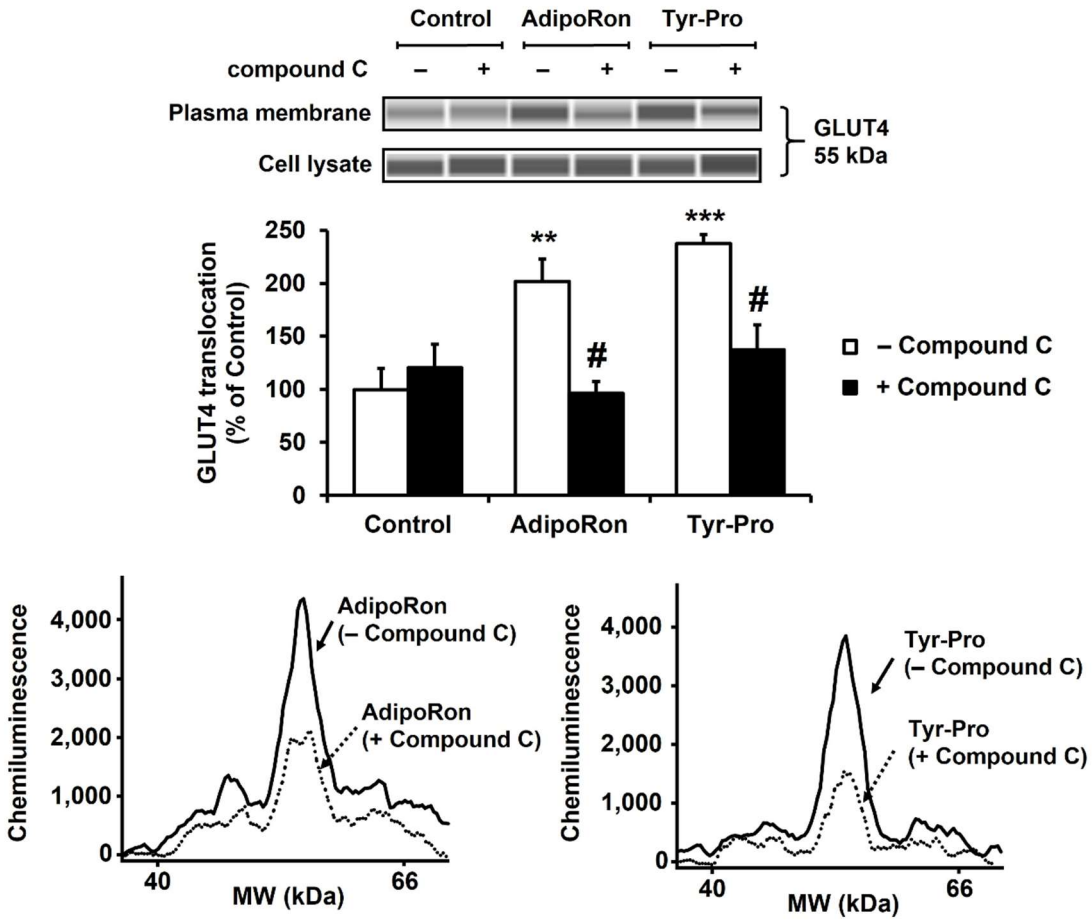

Fig. 2-11. Effect of YP on GLUT4 translocation in L6 myotubes.

The levels of GLUT4 in L6 myotubes treated with AdipoRon (0.1 μM, 0.5 h) or YP (1 μM, 1 h) in the presence or absence of Compound C (20 μM) were measured by the WES analysis to evaluate the effect of YP on GLUT4 translocation in L6 myotubes. Results are displayed as virtual blot-like images and electropherograms. Results are presented as mean ± SEM (n = 3–5). Statistical differences were assessed by Dunnett's t-test. $^{**}p < 0.01$, $^{***}p < 0.001$ *vs*. Control. Statistical differences between two groups in the presence or absence of Compound C were assessed by unpaired two-tailed Student's t-test. $^{\#}p < 0.05$.

3.5. *In silico* MD simulation analysis of YP-AdipoR1 docking complex

To clarify the structural requirement of YP for AdiopoR1 agonistic action, *in silico* MD simulations of AdipoRon, YP, PY, and WP with the seven-transmembrane receptor, AdipoR1, embedded in a CHARMM-GUI-aided POPC membrane were conducted. The MD simulations were performed at the two potential binding sites in AdipoR1 (sites 1/2), which can interact with adiponectin.[41] The complexes of AdipoRon, YP, PY, and WP with the AdipoR1 embedded in the POPC membrane provided constant protein RMSD values of 2.0–5.0 Å for MD simulations at sites 1/2, respectively (Figs. 2-12G and 2-13G). Considering a previous study[90] that rutin arachidonate bound to an ATPase calcium pump embedded in POPC system, exhibiting the stable RMSD value of 2.0–8.0 Å, the virtual systems developed in this study between targets and the AdipoR1 receptor were stably simulated. The complexed forms also revealed that the AdipoR1 agonistic YP dipeptide was stabilized at the inner position of each site in AdipoR1 (Figs. 2-12B and 2-13B), compared with the position of AdipoRon (Figs. 2-12A and 2-13A). At site 1, AdipoRon formed a hydrogen bond with His^{351}, hydrophobic interactions with Phe^{220}, Trp^{223}, Ser^{227}, Gly^{275}, Met^{300}, Phe^{303}, Tyr^{310}, and Leu^{358}, and π–π electron interactions with Tyr^{310} and Trp^{223} (Fig. 2-12E), whereas YP formed hydrogen bonds with Ser^{219}, Gly^{278}, Phe^{303}, and Tyr^{310}, hydrophobic interactions with Phe^{303} and Ala^{347}, and π–π electron interactions with Phe^{303} (Fig. 2-12F). At site 2, it was simulated that AdipoRon formed a hydrogen bond with Arg^{158}, hydrophobic interactions with

Phe^{163}, Pro^{166}, Phe^{173}, Gln^{359}, and Tyr^{363}, and π–π electron interactions with Phe^{173} and Tyr^{363} (Fig. 2-13E), whereas YP formed hydrogen bonds with Thr^{155} and Ser^{219}, hydrophobic bonds with Phe^{176}, Pro^{222}, and Phe^{352}, and π–π electron interactions with Phe^{176} (Fig. 2-13F).

The magnitude of intermolecular interactions between the four targets and AdipoR1 was assessed by the Gibbs free energy of binding (ΔG_{bind}) of the complex during the last 20 ns RMSD simulation (180–200 ns, 200 frames), using the MM-PBSA method. The apparent ΔG_{bind} of the AdipoRon-AdipoR1 complex at site 1 (-29.45 kcal/mol, Fig. 2-12H) and site 2 (-21.64 kcal/mol, Fig. 2-13H) was in good agreement with a potent AdipoR1 agonistic effect (Fig. 2-8), evidencing that AdipoRon, a molecularly designed AdipoR1 agonist, preferably binds to the both sites of the AdipoR1 receptor. Less ΔG_{bind} of WP (Figs. 2-12H and 2-13H), exerting no promoting effect on glucose uptake (Fig. 2-4), also validated the current MD simulation for the virtual ligand-AdipoR1 complex. The ΔG_{bind} of YP-AdipoR1 complex at site 1 (-11.59 kcal/mol) and site 2 (-13.32 kcal/mol) demonstrated the favorable agonistic action of YP towards the both sites of AdipoR1, similar to AdipoRon. The unexpected result that PY, with no *in vitro* bioactivity in L6 myotubes (Fig. 2-3), had a compatible ΔG_{bind} at site 1 (-8.72 kcal/mol) and site 2 (-8.35 kcal/mol) with those of YP acquired from *in silico* analysis. The conflicting results between *in vitro* and *in silico* experiments might be explained by the degradation (or enzymatic hydrolysis) of PY during the 1 h-glucose uptake experiments (Fig. 2-14).

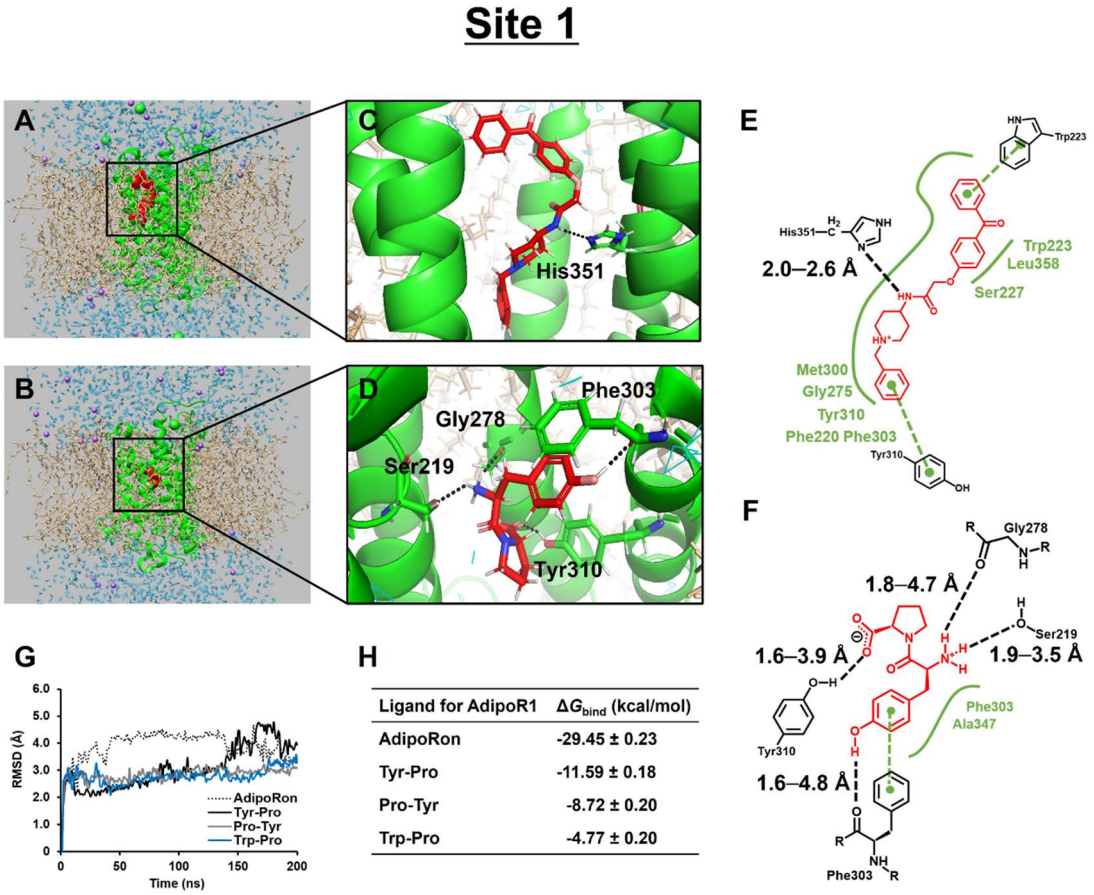

Ligand for AdipoR1	ΔG_{bind} (kcal/mol)
AdipoRon	-29.45 ± 0.23
Tyr-Pro	-11.59 ± 0.18
Pro-Tyr	-8.72 ± 0.20
Trp-Pro	-4.77 ± 0.20

Fig. 2-12. *In silico* MD simulation analyses at site 1.

MD simulation analyses of the AdipoRon-AdipoR1-POPC complex (A) and YP-AdipoR1-POPC complex (B) at site 1 (ligand, red; Na^+, green sphere; Cl^-, purple sphere; POPC, brown; water molecule, cyan) were performed. Binding conformations of AdipoRon (C) and YP complexes (D) at 200 ns were visualized (C atom, red; H atom, white; N atom, blue; O atom, pink). Intermolecular interactions of AdipoRon (E) and YP complexes (F) at 200 ns were visualized (hydrogen bond, black dashed line; hydrophobic interaction, green straight line; π–π electron interaction, green dashed line). Protein backbone root-mean-square deviation (RMSD) values were computed for 200 ns (G). The Gibbs free energy of binding values, ΔG_{bind} (kcal/mol) were estimated for 180–200 ns (H).

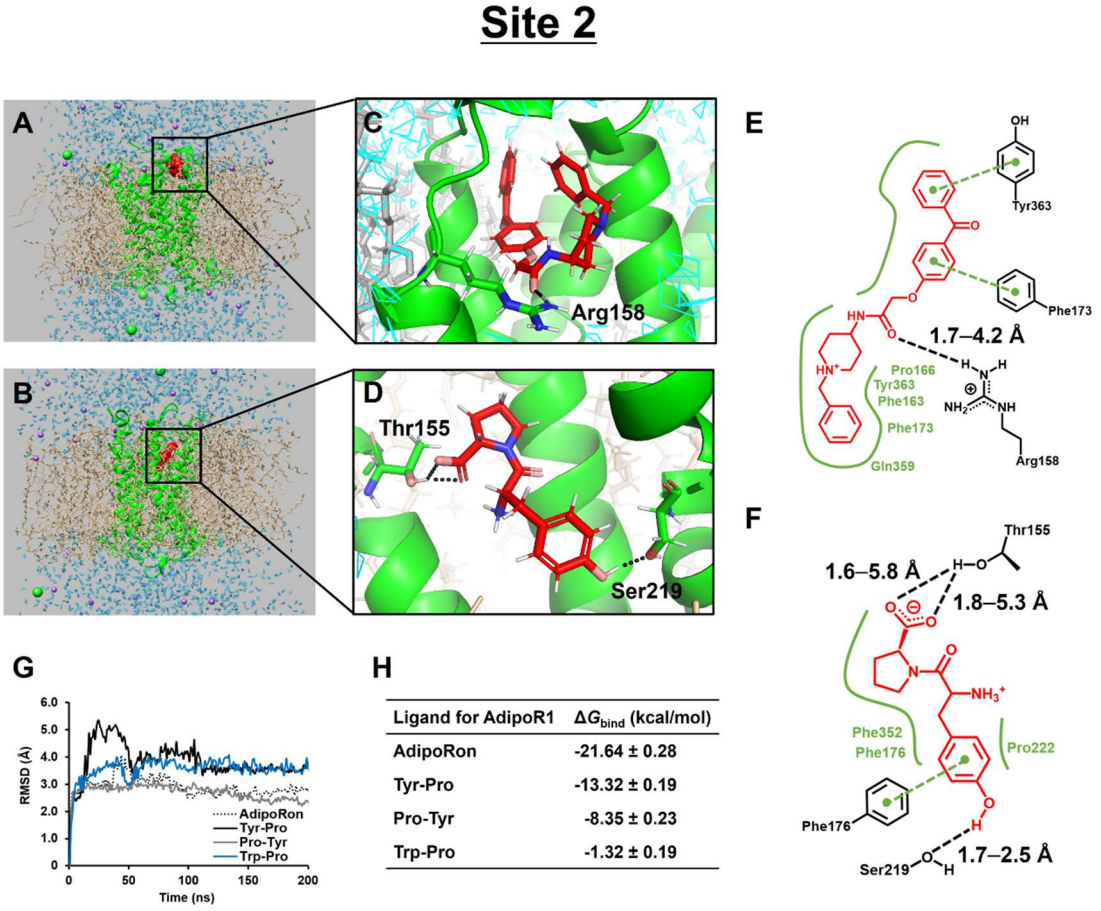

Ligand for AdipoR1	ΔG_{bind} (kcal/mol)
AdipoRon	-21.64 ± 0.28
Tyr-Pro	-13.32 ± 0.19
Pro-Tyr	-8.35 ± 0.23
Trp-Pro	-1.32 ± 0.19

Fig. 2-13. *In silico* MD simulation analyses at site 2.

MD simulation analyses of the AdipoRon-AdipoR1-POPC complex (A) and YP-AdipoR1-POPC complex (B) at site 2 (ligand, red; Na^+, green sphere; Cl^-, purple sphere; POPC, brown; water molecule, cyan) were performed. Binding conformations of AdipoRon (C) and YP complexes (D) at 200 ns were visualized (C atom, red; H atom, white; N atom, blue; O atom, pink). Intermolecular interactions of AdipoRon (E) and YP complexes (F) at 200 ns were visualized (hydrogen bond, black dashed line; hydrophobic interaction, green straight line; π–π electron interaction, green dashed line). Protein backbone root-mean-square deviation (RMSD) values were computed for 200 ns (G). The Gibbs free energy of binding values, ΔG_{bind} (kcal/mol) were estimated for 180–200 ns (H).

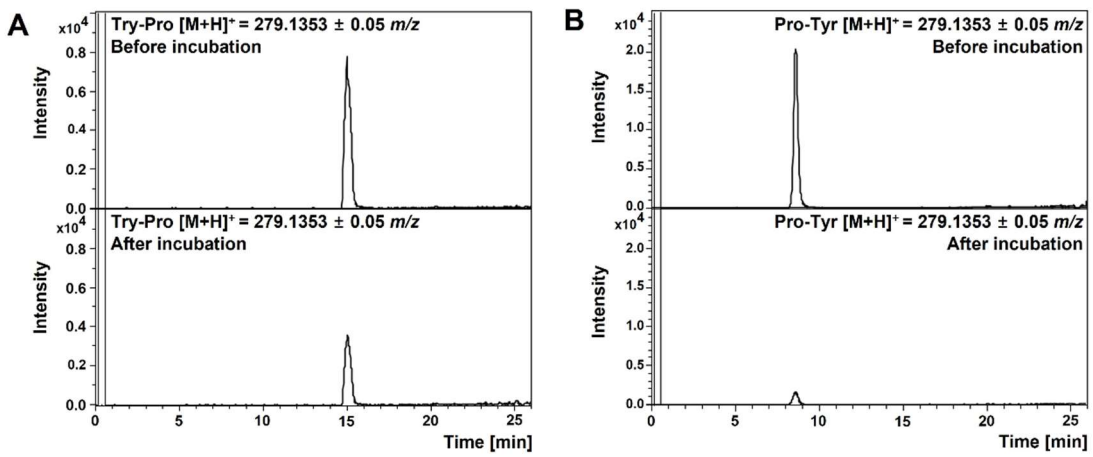

Fig. 2-14. Evaluation of stability of YP and PY in the L6 cell medium.

LC-TOF/MS chromatograms in the extracted ion-chromatograms mode of dipeptides (279.1353 *m/z* for YP (A) and 279.1353 *m/z* for PY (B)) at 1 μM were acquired from cell medium solution before and after glucose uptake experiments for 1 h.

High ΔG_{bind} of < -8 kcal/mol for YP as well as PY, estimated by the MM-PBSA method, may be explained by the key-player, Tyr, in their sequences for binding to AdipoR1 sites, in which the presence of a hydroxyl group and an aromatic ring of Tyr may greatly influence the high stability of the Pro-dipeptides at each site of AdipoR1 by an intermolecular hydrogen bond and a π–π electron interaction (Figs. 2-12F, 2-13F, 2-15E, and 2-15K). The poor ΔG_{bind} of > -5 kcal/mol for WP may be due to the lack of the above two intermolecular interactions between Trp and the receptor at the two binding sites (Figs. 2-15F and 2-15L).

Taken together, the *in silico* MD simulation analyses of YP, PY, and WP at the sites of AdipoR1 revealed that the intermolecular interactions between Tyr and the sites would elicit the AdipoR1 agonistic effect of Pro-dipeptides.

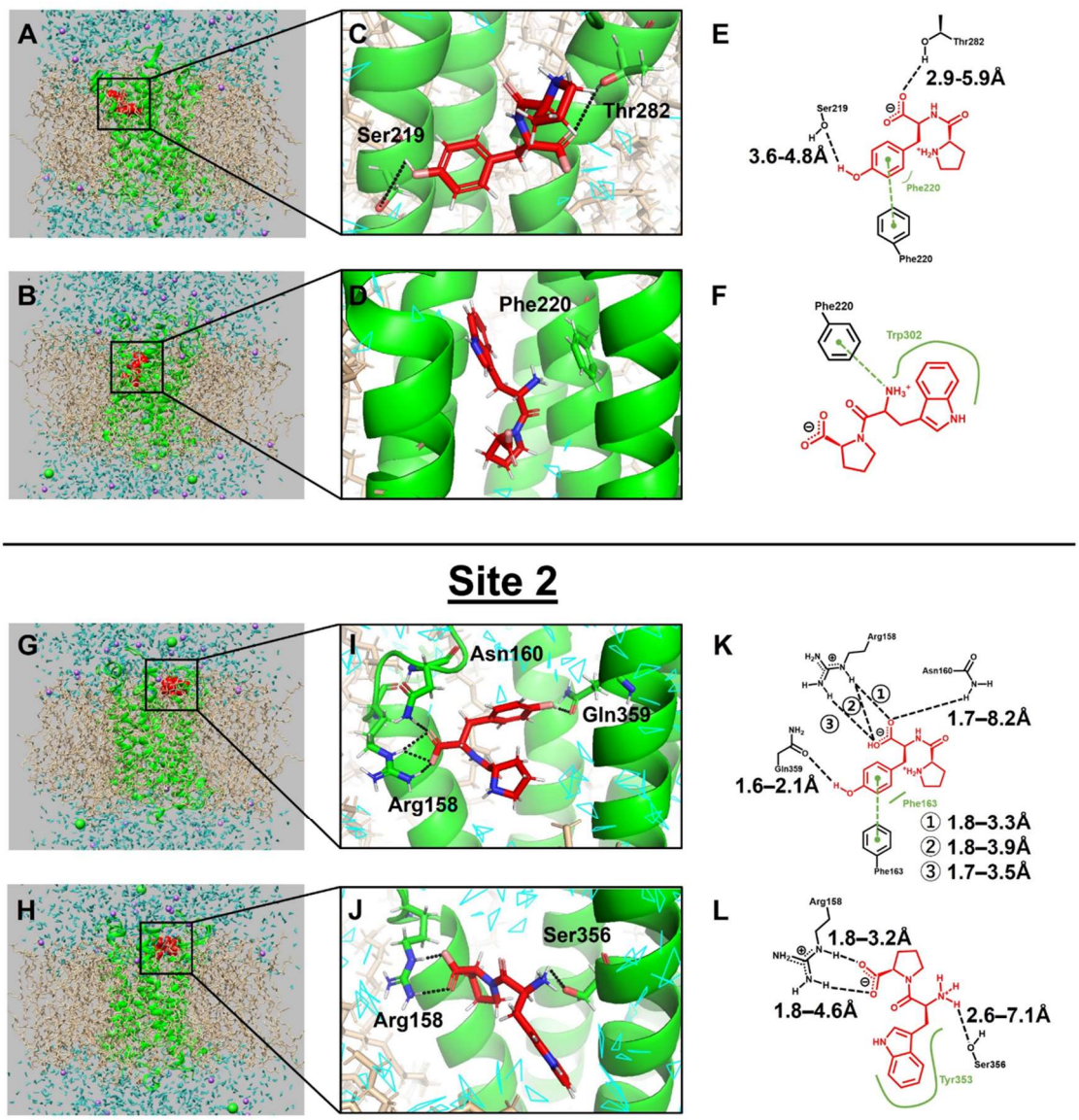
Site 1
A
B
C
Ser219
Thr282
D
Phe220
E
Thr282
2.9-5.9Å
Ser219
3.6-4.8Å
Phe220
Phe220
F
Phe220
Trp302
NH3+
NH
Site 2
G
H
I
Asn160
Gln359
Arg158
J
Ser356
Arg158
K
Arg158
Asn160
1.7–8.2Å
Gln359
1.6–2.1Å
Phe163
① 1.8–3.3Å
② 1.8–3.9Å
③ 1.7–3.5Å
Phe163
L
Arg158
1.8–3.2Å
1.8–4.6Å
2.6–7.1Å
Ser356
Tyr353

Fig. 2-15. *In silico* MD simulation analyses at sites 1/2.

MD simulation analyses of the PY-AdipoR1-POPC complex (A) and WP-AdipoR1-POPC complex (B) at site 1 (ligand, red; Na^+, green sphere; Cl^-, purple sphere; POPC, yellow; water molecule, cyan) were performed. Binding conformations of PY (C; T = 196 ns) and WP complexes (D; T = 193 ns) were visualized (C atom, red; H atom, white; N atom, blue; O atom, pink). Intermolecular interactions of PY (E; T = 196 ns) and WP complexes (F; T = 193 ns) were visualized (hydrogen bond, black dashed line; hydrophobic interaction, green straight line; π–π electron interaction, green dashed line).

MD simulation analyses of the PY-AdipoR1-POPC complex (G) and WP-AdipoR1-POPC complex (H) at site 2 (ligand, red; Na^+, green sphere; Cl^-, purple sphere; POPC, yellow; water molecule, cyan) were performed. Binding conformations of PY (I) and WP complexes (J) at 200 ns were visualized (C atom, red; H atom, white; N atom, blue; O atom, pink). Intermolecular interactions of PY (K) and WP complexes (L) at 200 ns were visualized (hydrogen bond, black dashed line; hydrophobic interaction, green straight line; π–π electron interaction, green dashed line).

2.4. Summary

Chapter II demonstrates a dipeptide YP exhibiting AdipoR1 agonistic action by binding to AdipoR1 by *in vitro* and *in silico* experiments. The dipeptide YP, present in soybean hydrolysate, was evidenced to promote the glucose uptake in rat skeletal muscle L6 cells through the AdipoR1-mediated activation of AMPK/GLUT4 translocation. Moreover, *in silico* MD simulation analysis using a virtual phospholipid membrane revealed that the dipeptide YP was stably positioned in the potential two binding pockets of AdipoR1 receptor. In conclusion, the dipeptide YP may be a novel candidate for the prevention of insulin-independent T2DM as an adiponectin-like "orally-active" food compound.

Chapter III

Adiponectin receptor agonistic action of soybean tripeptides by *in vitro* rat skeletal muscle L6 cells and *in silico* analyses

1. Introduction

Currently approved anti-diabetic drugs that regulate blood glucose levels, such as biguanides, sulfonylureas, thiazolidinediones, α-glucosidase inhibitors, and dipeptidyl peptidase-4 inhibitors, have undesirable side effects.[91] Various food-derived compounds involving biologically active peptides have displayed physiological functions that are potentially valuable in managing and preventing insulin-independent type 2 diabetes mellitus (T2DM).[92-93] Several good candidate anti-diabetic food compounds have been found. These include tripeptide Ile-Pro-Pro that activates liver kinase B1 (LKB1)/adenosine monophosphate-activated protein kinase (AMPK)/glucose transporter 4 (GLUT4) translocation[74] and cereal tripeptides that include Ile-Gln-Pro, Ile-

Pro-Gln, Val-Pro-Glu, and Val-Glu-Pro,[73] which activate insulin-independent AMPK/GLUT4 translocation. However, the mechanism by which these peptides activate signaling for GLUT4 translocation remains still unclear.

As described in **Chapter II,** a novel AdipoR1 agonistic dipeptide Tyr-Pro (YP) was elucidated according to the structural similarity with AdipoRon, and it was confirmed by using *in silico* molecular dynamics (MD) simulation that YP preferentially binds to adiponectin receptor 1 (AdipoR1). This simulation revealed that elevated adiponectin-like AMPK/GLUT4 translocation was induced in L6 myotubes. The MD simulation analysis also indicated that YP was stably located, with a high binding affinity of Gibbs free energy of binding (ΔG_{bind}) < -10 kcal/mol, at the inner side of the two binding sites 1/2 of the seven-transmembrane receptor, AdipoR1 that was embedded in a virtual 1-palmitoyl-2-oleoyl-phosphatidylcholine (POPC) membrane.

The present study was undertaken to determine whether alternative food-derived peptides can have anti-T2DM via adiponectin-like AdipoR1 stimulation. Soybean proteins were targeted to study because the intake of soybean proteins is reportedly effective in preventing T2DM, and they possess seventeen YP-related tripeptide sequences (Table 3-1). Once promising tripeptide candidates were found in the soybean protein sequence,[94] the next aim was to clarify the molecular interaction between ligand tripeptide and AdipoR1 protein using the CHARMM-GUI-aided MD simulation analysis.[80]

Table 3-1. Tripeptides containing Tyr and Pro residues in the sequence of soybean proteins.

Sequence	Position in soybean proteins
GYP	β-conglycinin α subunit 2 (511–513), β-conglycinin α' subunit (527–529)
AYP	β-conglycinin α subunit 1 (345–347), β-conglycinin β subunit 1 (345–347), β-conglycinin β subunit 2 (345–347)
EYP	Glycinin-G4 (196–198)
IYP	Glycinin-G1 (103–105)
PYP	Glycinin-G4 (87–89), Glycinin-G5 (88–90)
SYP	Glycinin-G5 (294–296)
YLP	Glycinin-G5 (86–88)
YNP	Glycinin-G1 (334–336), Glycinin-G2 (324–326), Glycinin-G4 (402–404)
YQP	Glycinin-G3 (192–194)
YSP	Glycinin-G4 (85–87, 438–440), Glycinin-G5 (404–406)
YPG	Glycinin-G1 (104–106)
YPE	Glycinin-G4 (197–199)
YPF	β-conglycinin α subunit 1 (346–348), β-conglycinin β subunit 1 (346–348), β-conglycinin β subunit 2 (346–348)
YPQ	Glycinin-G5 (89–91)
YPR	Glycinin-G4 (88–90)
YPV	β-conglycinin α subunit 2 (512–514), β-conglycinin α' subunit (528–530)
YPP	Glycinin-G5 (295–297)

2. Materials and Methods

2.1. Materials

AdipoRon was obtained from Cayman Chemical and dimethyl sulfoxide (DMSO) was obtained from Sigma-Aldrich. Dulbecco's modified Eagle's medium (DMEM), fetal bovine serum (FBS), horse serum (HS), and Opti-minimum essential medium (Opti-MEM) were purchased from Gibco. α-minimum essential medium (α-MEM) was obtained from FUJIFILM Wako Pure Chemical Co. and 2-[*N*-(7-nitrobenz-2-oxa-1,3-diazol-4-yl) amino]-2-deoxy-D-glucose (2-NBDG) was obtained from Invitrogen. YP and Tyr-Pro-Pro (YPP) were purchased from Kokusan Chemical Co. and Watanabe Chemical Industries (Hiroshima, Japan), respectively. Other tripeptides were synthesized by 9-fluorenylmethoxycarbonyl-based solid-phase synthesis method[95]: Gly-Tyr-Pro (GYP), Ala-Tyr-Pro (AYP), Glu-Tyr-Pro (EYP), Ile-Tyr-Pro (IYP), Pro-Tyr-Pro (PYP), Ser-Tyr-Pro (SYP), Tyr-Gly-Pro (YGP), Tyr-Leu-Pro (YLP), Tyr-Asn-Pro (YNP), Tyr-Gln-Pro (YQP), Tyr-Ser-Pro (YSP), Tyr-Pro-Gly (YPG), Tyr-Pro-Glu (YPE), Tyr-Pro-Phe (YPF), Tyr-Pro-Gln (YPQ), Tyr-Pro-Arg (YPR), and Tyr-Pro-Val (YPV). Their purity (>90%) and sequences were confirmed by high-performance liquid chromatography (HPLC; LC-10AD, Shimadzu, Kyoto, Japan) and ion-trap mass spectrometry (IT-MS; Esquire6000, Bruker Daltonics, Bremen, Germany). Other chemicals were used without further purification.

2.2. Cell culture

The procedure and conditions for L6 cell culture were the same as described in **Chapter II**. Briefly, L6 myoblasts were grown in 10% FBS/DMEM, and differentiated in 2% HS/DMEM for at least 5 days. Prior to performing each experiment, L6 myotubes were serum-starved in 0.2% bovine serum albumin (BSA)/α-MEM for 18 h.

2.3. Glucose uptake assay

Glucose uptake experiments in L6 myotubes were performed as described in **Chapter II** with slight modifications. Briefly, L6 myotubes were incubated with 100 μL of the respective peptide sample (0.01 μM, 30 min). AdipoRon (0.1 μM, 30 min) was used as a positive control. The myotubes were then incubated with 100 μL of 100 μM 2-NBDG solution for 30 min. After being washed with Krebs–Ringer phosphate HEPES (KRPH) buffer, the fluorescence intensity of 2-NBDG was measured at excitation and emission wavelengths of 480 and 535 nm, respectively, using a Wallac 1420 ARVO MX multilabel counter (PerkinElmer, Waltham, MA, USA).

2.4. Knockdown of AdipoR1 using siRNA transfection

According to the method described in **Chapter II**, L6 cells were transfected with either AdipoR1 siRNA (sc-156024, Lot: G1321; Santa Cruz Biotechnology) or negative control siRNA (sc-37007, Lot: G2021; Santa Cruz Biotechnology). Briefly, the cells were transfected for 6 h with 20 nM siRNA dissolved in Opti-MEM, using a Hiperfect transfection reagent (QIAGEN). After differentiation, the cells were re-transfected using the same method.

As described in **Chapter II**, the siRNA-transfected cells were lysed in radioimmunoprecipitation assay (RIPA) buffer containing protease and phosphatase inhibitors and centrifuged (20,000 × *g*, 20 min, 4°C) to obtain the cell lysate. The cell lysate was subjected to WES analysis to detect the level of AdipoR1.

2.5 GLUT4 translocation assay

The experiment of GLUT4 translocation were the same as described in **Chapter II**. Briefly, the differentiated L6 myotubes were treated with either YPG (0.1 μM, 30 min) or YPP (0.1 μM, 30 min). The sample-treated cells were suspended in ice-cold lysis buffer (50 mM Tris-HCl, 0.5 mM dithiothreitol, pH 8.0) containing 0.1% Nonidet P-40 (NP-40), and protease and phosphatase inhibitors, and homogenized. The homogenate was then centrifuged (1,000 × *g*, 10 min, 4°C) to obtain a pellet. The pellet was suspended in the lysis buffer with the same inhibitors, kept on ice for 10 min, and then centrifuged (1,000 × *g*, 10 min, 4°C). The resulting pellet was re-suspended in the lysis buffer containing 1% NP-40 and the same inhibitors on ice for 1 h with intermittent agitation. After centrifugation (20,000 × *g*, 20 min, 4°C), the supernatant was gathered as the plasma membrane.

To extract the whole cell lysate, part of the homogenate prepared as described above was added with an equal volume of 2 × RIPA buffer with the same inhibitors and kept on ice for 1 h with intermittent agitation. After centrifugation (20,000 × *g*, 20 min, 4°C), the supernatant was collected as the cell lysate. The extracted samples were subjected to WES analysis to detect the level of GLUT4 translocation.

2.6. The WES analysis

According to the method described in **Chapter II,** the lysate samples were subjected to WES analysis for the measurement of AdipoR1 and GLUT4. The sample protein concentrations used were as follows: 1.0 μg/μL of cell lysate for AdipoR1 and 0.5 μg/μL of cell lysate and 2.0 μg/μL of plasma membrane for GLUT4. The samples were denatured for 5 min at 95°C (for AdipoR1) and for 20 min at 37°C (for GLUT4), respectively. The primary antibodies used were as follows: AdipoR1 (1:50 dilution, anti-rabbit, ab126611, Lot: GR3309856-1; Abcam) and GLUT4 (1:10 dilution, anti-mouse, 2213S, Lot: 2022; Cell Signaling Technology). A total protein assay was conducted to normalize the target protein signal using a pentafluorophenyl ester-biotin labeling reagent. Following plate loading, electrophoresis and immunodetection were performed in a fully automated capillary system. The data were displayed as virtual blot-like images and electropherograms based on the molecular weight by a Compass software (ProteinSimple Co.). Protein expression of AdipoR1 and GLUT4 was normalized using the electropherogram peak area of total protein applied in each lane, and the date were expressed as the ratios against control.

2.7. Determination of tripeptide in soybean hydrolysate by LC-TOF/MS

The amount of tripeptide in a commercially available soybean hydrolysate (Hinute AM, Fuji Oil Co., Tokyo, Japan) was estimated according to a liquid chromatography-time-of-flight/mass spectrometry (LC-TOF/MS)-aided standard addition method to avoid interference by the protein hydrolysate matrix during the MS detection.[96] The hydrolysate solution (10 mg/mL) was spiked with YPG (20 μg/g) and YPP (20, 40, and 75 μg/g) and mixed vigorously. After passing through a 0.2-μm-polytetrafluoroethylene membrane filter, 20 μL of the filtrate was injected into a LC-TOF/MS. The chromatographic separation was conducted by an Agilent 1200 series HPLC system that was equipped with a Cosmosil $5C_{18}$-AR-II column (2.0 × 150 mm, Nacalai Tesque) and eluted with a linear gradient of water containing 0.1% formic acid to acetonitrile containing 0.1% formic acid (20 min) at a flow rate of 0.2 mL/min at 40°C. TOF/MS analysis was conducted using a Bruker micrOTOF-II MS equipment in electrospray ionization (ESI)-positive ion mode ($[M + H]^+$, 336.1554 *m/z* for YPG and 376.1867 *m/z* for YPP). The MS parameters were set as follows: drying N_2 gas, 8.0 L/min; drying temperature, 200°C; nebulizer pressure, 1.6 bar; capillary voltage, 4500 V; and mass range, 100–1000 *m/z*. A calibration solution (10 mM sodium formate in 50% acetonitrile) was injected at the beginning of each run, and all spectra were internally calibrated. Data acquisition and analysis were performed using a Bruker Data Analysis ver. 4.0.

2.8. Molecular docking and MD simulation

In silico experiment was performed according to the method described in **Chapter II.** Tripeptides, YPG and YPP for docking study were constructed using a Chimera ver. 1.15. As described in Fig. 2-2 of **Chapter II**, AdipoR1 structure (PDB ID 3WXV) was utilized to create an appropriate protein model for ligand docking. Unnecessary parts (nanobodies) were removed from the initial structure using a PyMOL ver. 2.4.1. Missing amino acid residues (Pro^{159}, Asn^{160}, Gly^{298}, and Gln^{299}) were inserted using a MODELLER ver. 9.23. A complete structure was obtained by adding a missing zinc ion to the MODELLER-reconstructed AdipoR1 protein. Virtual docking of the ligand tripeptides to the two reported pockets (sites 1/2) of AdipoR1[41] was performed using AutoDock Tools ver. 1.5.7. The grid-box parameters for docking were same as listed in Table 2-1 of **Chapter II**.

MD simulations of AdipoR1 anchored in a virtual phospholipid membrane were performed using an AMBER ver. 18.[85] A virtual POPC bilayer solvated by transferable intermolecular potential with three points (TIP3P) water with 150 mM NaCl was created using the CHRAMM-GUI protocol.[80] The AMBER ff14SB[82] and lipid14[83] force fields were used to construct the tripeptides and POPC, respectively. Energy minimization and equilibration of the tripeptide-AdipoR1 complex in the POPC membrane were implemented at 310 K and a pressure of 1.0 atm for 200 ns. The protein backbone root-mean-square deviation (RMSD) of the complex in POPC was used to assess the stability of

the virtual system in this study.

After the MD simulation, to evaluate the binding affinities between the tripeptide and AdipoR1 in the POPC system, the Gibbs free energy of binding (ΔG_{bind}) was estimated during 180–200 ns of the simulation, using the molecular mechanics Poisson–Boltzmann surface area (MM-PBSA) method,[86] as described equation in **Chapter II**. Intermolecular interactions between the ligand and AdipoR1 were observed, and hydrogen bonds, hydrophobic, and π–π electron interactions in the complex were visualized using a Proteins*Plus* server. The hydrogen bond distances were calculated during 180–200 ns simulation using a Chimera ver. 1.15. Furthermore, per-residue decomposition analysis[97] was performed to elucidate the energetic contribution of each amino acid residue to ligand binding.

2.9. Statistical analysis

Results are presented as mean ± standard error of the mean (SEM). Statistical differences within groups were assessed by one-way analysis of variance (ANOVA), followed by Dunnett's *t*-test for post hoc analysis. Statistical differences between two groups were evaluated using unpaired two-tailed Student's *t*-test. A $p < 0.05$ was regarded as statistically significant. All analyses were performed using GraphPad Prism ver. 5.0 (La Jolla, CA, USA).

3. Results and Discussion

3.1. Glucose uptake ability of YP-related tripeptides in L6 myotubes

The potential of YP-related tripeptides containing Gly (GYP, YGP, and YPG) to promote glucose uptake in L6 myotubes was investigated using 2-NBDG uptake assay, since the dipeptide YP is known to promote glucose uptake via an AdipoR1 agonistic effect in **Chapter II**. Among the three tripeptides, YPG caused a significant increase in 2-NBDG uptake in L6 myotubes (153 ± 18%, $p < 0.05$), which was comparable with that of the skeleton dipeptide YP (157 ± 8%, $p < 0.05$) (Fig. 3-1). This observation suggests that tripeptide YPG, just like dipeptide YP, may have the potential to promote glucose uptake. Furthermore, elongation of the C-terminus of the YP skeleton by Gly does not affect the potential of YP to promote glucose uptake. In contrast, elongation of the N-terminus and at the middle of the YP sequence by inserting Gly in between caused the disappearance of YP's ability to promote glucose uptake, suggesting that tripeptides with the Y-P-X sequence (X = a given amino acid) would be a leading candidate for the promotion of glucose uptake in L6 myotubes. Next, we examined the potential of YPG to promote 2-NBDG uptake by L6 myotubes. The effect of YPG on 2-NBDG uptake was examined as a function of concentration (0.01, 0.1, or 1 μM) for 30 min. A significant ($p < 0.05$) promoting response of YPG was obtained at a concentration of more than 0.1 μM when L6 myotubes were incubated for 30 min (Fig. 3-2). Thus, further screening experiments for tripeptides were performed at 0.1 μM concentration for 30 min.

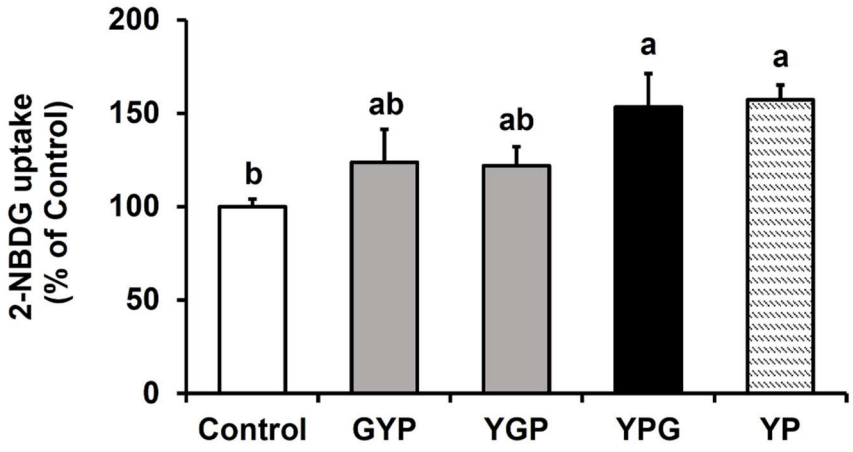

Fig. 3-1. Effect of tripeptides composed of Gly, Tyr, and Pro on glucose uptake in L6 myotubes.

L6 myotubes were incubated with 1 μM tripeptides (GYP, YGP, and YPG) or 1 μM YP (positive control) for 1 h. Results are presented as mean ± SEM (n = 5–6). Statistical differences were assessed by Tukey-Kramer test. Means with different letters represent statistically different at $p < 0.05$.

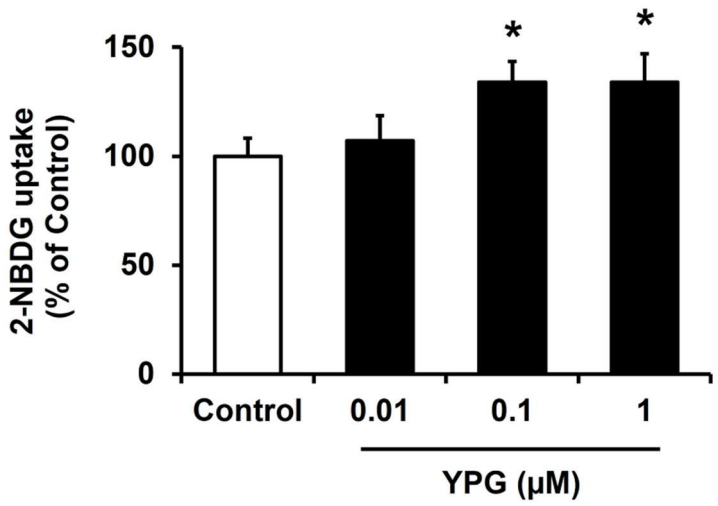

Fig. 3-2. Concentration-effect of YPG on glucose uptake in L6 myotubes.

L6 myotubes were incubated with 0.01, 0.1, or 1 μM YPG for 30 min to evaluate the effect of YPG concentration on 2-NBDG uptake. Results are presented as mean ± SD (n = 5 or 6). Statistical differences were assessed by Dunnett's t-test. *$p < 0.05$ *vs*. Control.

3.2. Glucose uptake ability of Y-P-X tripeptides in soybean proteins in L6 myotubes

As listed in Table 1-1, a total of 17 tripeptides with YP sequences were found in the β-conglycinin and glycinin that were main storage proteins of soybean.[98] However, considering the finding that Y-P-X may potentially promote glucose uptake (Fig. 3-1), further glucose uptake experiments in L6 myotubes were performed focusing on the seven Y-P-X soybean tripeptides (Table 1-1). As shown in Fig. 3-3, four tripeptides of YPG, YPE, YPP, and YPQ at 0.1 μM significantly ($p < 0.05$) promoted 2-NBDG uptake by L6 myotubes, similar to 0.1 μM AdipoRon (YPG, 140 ± 7%; YPE, 141 ± 11%; YPP, 145 ± 9%; YPQ, 143 ± 9%; AdipoRon, 163 ± 23%). In contrast, Phe, Arg, and Val positioned at the C-terminus of YP had no effect. The absence of significant 2-NBDG uptake mediated by 0.1 μM YP suggested that the tripeptides mediated higher glucose uptake than that by the model dipeptide YP. These findings agree with Kim *et al*.,[99] who reported the peptide-length-dependent promotion of glucose uptake by oligo- (up to hexa-) peptides in adipocytes. No significant glucose uptake was observed in response to the soybean X-Y-P (Fig. 3-4) and Y-X-P tripeptides (Fig. 3-5), as predicted from the results in Fig. 3-1.

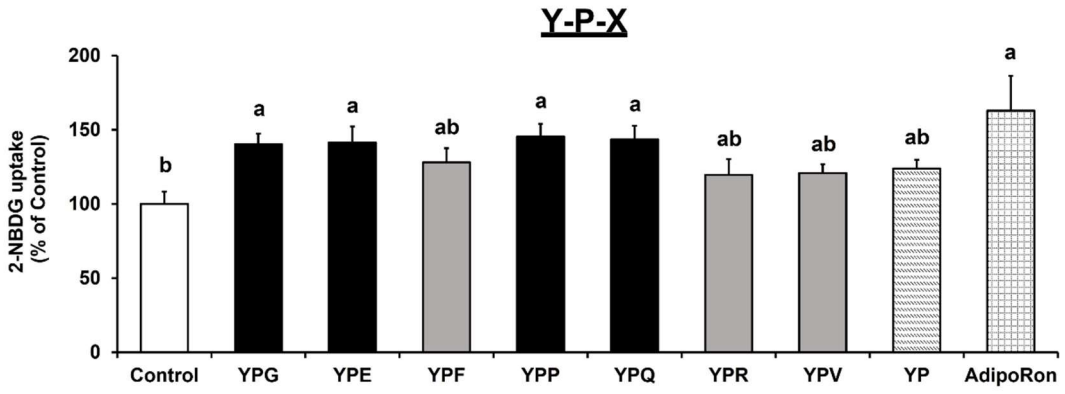

Fig. 3-3. The ability of Y-P-X tripeptides to promote glucose uptake in L6 myotubes.

The tripeptides were designed based on the Y-P-X sequence, where X represents the following amino acids: G, Gly; E, Glu; F, Phe; P, Pro; Q, Gln; R, Arg; V, Val. L6 myotubes were incubated with tripeptides, YP, or AdipoRon at a concentration of 0.1 μM for 30 min. Results are presented as mean ± SEM (n = 5–6). Statistical differences were assessed by Tukey-Kramer test. Means with different letters represent statistically different at $p < 0.05$.

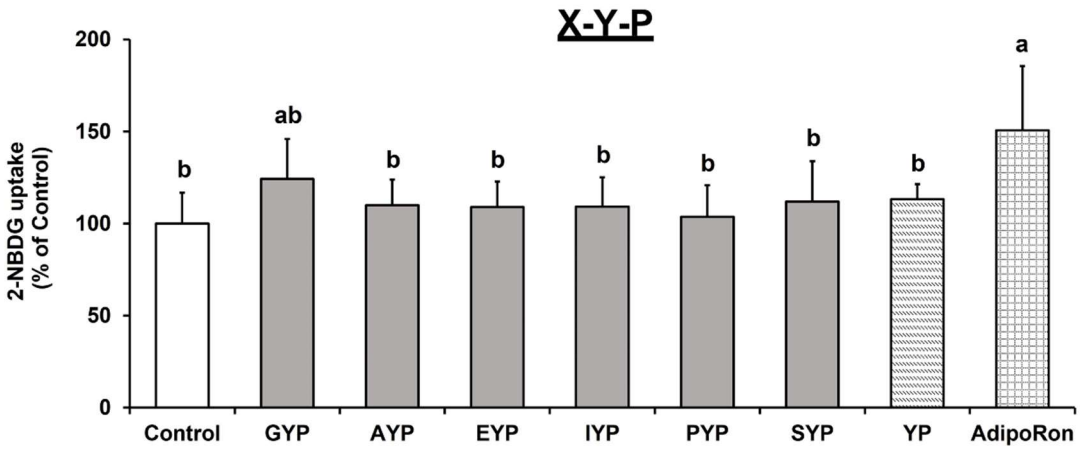

Fig. 3-4. The ability of X-Y-P tripeptides to promote glucose uptake in L6 myotubes.

The tripeptides were designed based on the X-Y-P sequence, where X represents the following amino acids: G, Gly; A, Ala; E, Glu; I, Ile; P, Pro; S, Ser. L6 myotubes were incubated with tripeptides, YP, or AdipoRon at a concentration of 0.1 μM for 30 min. Results are presented as mean ± SEM (n = 5–6). Statistical differences were assessed by Tukey-Kramer test. Means with different letters represent statistically different at $p < 0.05$.

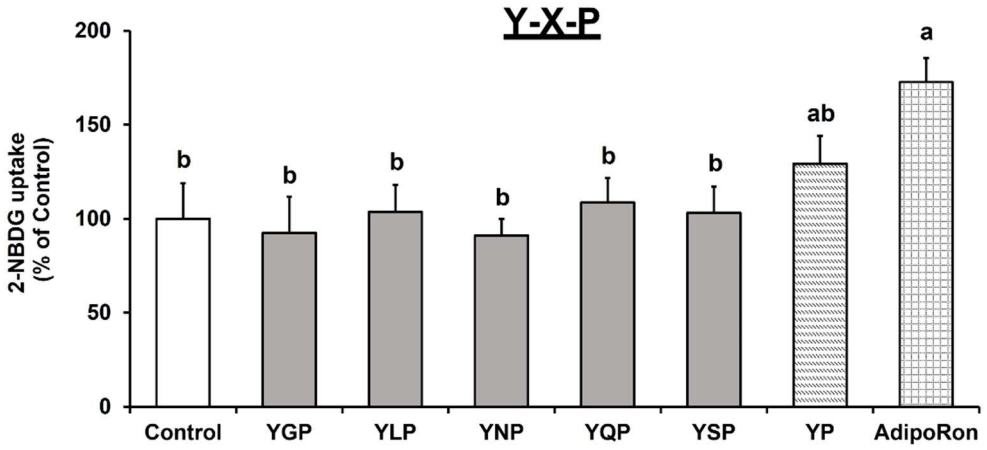

Fig. 3-5. The ability of Y-X-P tripeptides to promote glucose uptake in L6 myotubes.

The tripeptides were designed based on the Y-X-P sequence, where X represents the following amino acids: G, Gly; L, Leu; N, Asn; Q, Gln; S, Ser. L6 myotubes were incubated with tripeptides, YP, or AdipoRon at a concentration of 0.1 μM for 30 min. Results are presented as mean ± SEM (n = 5–6). Statistical differences were assessed by Tukey-Kramer test. Means with different letters represent statistically different at $p < 0.05$.

3.3. Involvement of AdipoR1 in tripeptides-induced glucose uptake in L6 myotubes

To confirm whether the 2-NBDG uptake promoted by the four tripeptides depicted in Fig. 3-3 was caused by an adiponectin-like action, similar to the action of the YP dipeptide skeleton, AdipoR1 expression was knocked down in L6 myotubes by silencing AdipoR1 siRNA (Fig. 3-6). In AdipoR1-siRNA-transfected L6 cells, 2-NBDG uptake in response to YPG, YPP, and AdipoRon at 0.1 μM was significantly ($p < 0.05$) abrogated (Fig. 3-7). These results strongly suggested that the tripeptides YPG and YPP that showed higher promoting potential than YP (Fig. 3-3) can be considered as novel AdipoR1 agonistic peptides.

The lack of the influence of AdipoR1-knockdown on the ability of YPQ and YPE to promote glucose uptake in L6 myotubes (Fig. 3-7) suggest that it they did not lie in the AdipoR1-related signaling axis, but in another glucose incorporation axis (e.g., PHT1-mediated LKB1/GLUT4 translocation[60]). Further studies are required to clarify the mechanisms underlying the YPQ- and YPE-mediated glucose uptake using separate cell line experiments.

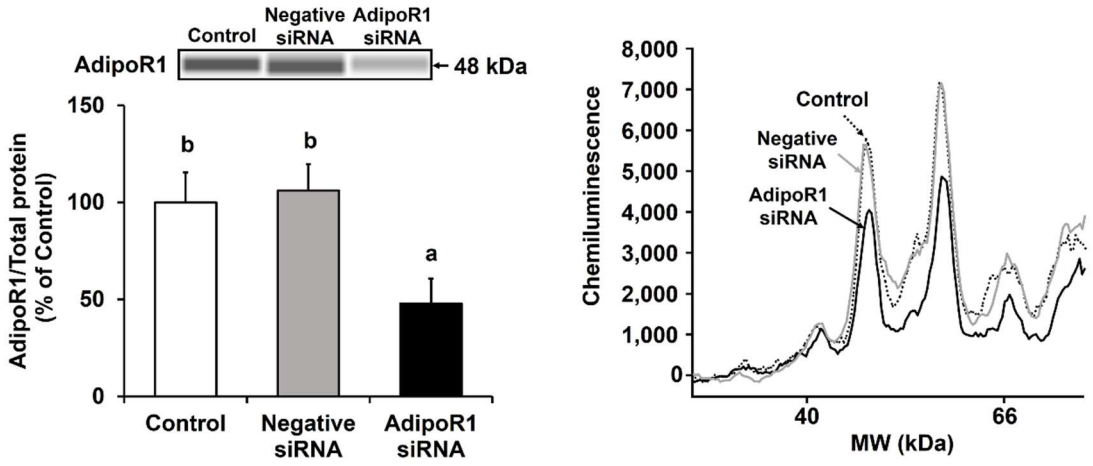

Fig. 3-6. AdipoR1-knockdown in L6 myotubes by siRNA transfection.

The level of AdipoR1 was measured by the WES analysis in AdipoR1-knockdown L6 myotubes by AdipoR1-specific siRNA transfection. Results are displayed as virtual blot-like images and electropherograms. Results are presented as mean ± SEM ($n = 4$). Statistical differences were assessed by Tukey-Kramer test. Means with different letters represent statistically different at $p < 0.05$.

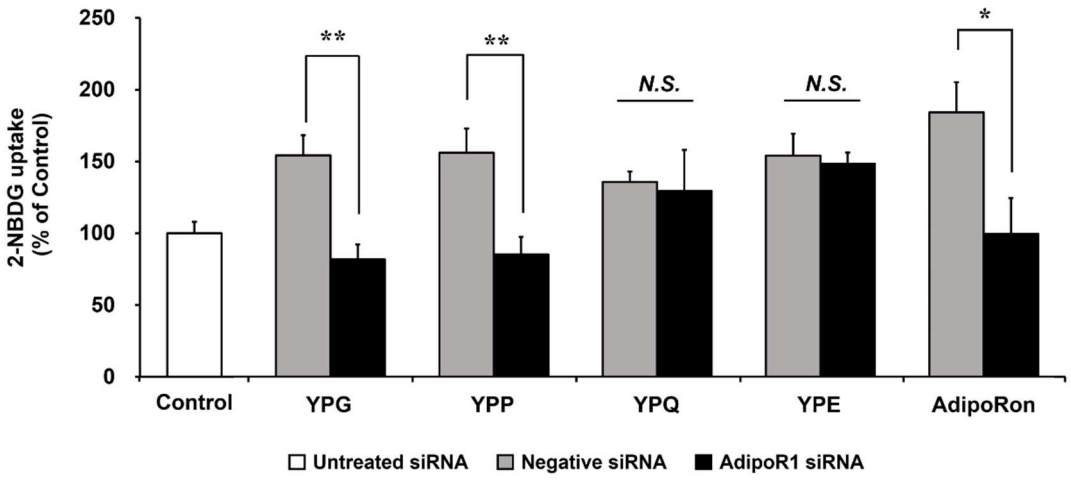

Fig. 3-7. Involvement of the AdipoR1 in promoting glucose uptake by tripeptides in L6 myotubes.

The knockdown L6 myotubes were incubated with 0.1 μM tripeptides (YPG, YPP, YPQ, and YPE) or 0.1 μM AdipoRon for 30 min to evaluate the effect of AdipoR1-knockdown in L6 myotubes on the promotion of 2-NBDG uptake by tripeptides. Results are presented as mean ± SEM (n = 5–6). Statistical differences between negative and AdipoR1 siRNA groups were assessed by unpaired two-tailed Student's t-test. $^{*}p < 0.05$, $^{**}p < 0.01$; *N.S.*, no significant difference at $p > 0.05$.

3.4. Effect of tripeptides on GLUT4 translocation in L6 myotubes

To clarify the mechanism of the promoting glucose uptake of YPP, GLUT4 translocation cascade in L6 myotubes was investigated. Fig. 3-8 revealed that the GLUT4 expression in plasma membrane of L6 myotubes was significantly ($p < 0.05$) promoted by both YPG and YPP. This observation indicated that both YPG and YPP may promote glucose uptake via the AdipoR1-mediated GLUT4 translocation pathway in L6 myotubes.

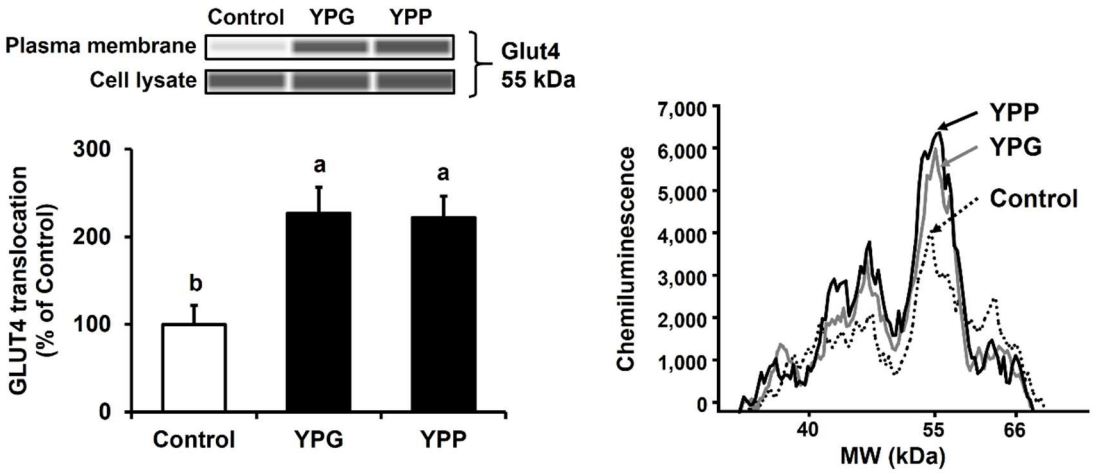

Fig. 3-8. Effect of tripeptides on GLUT4 translocation in L6 myotubes.

The levels of GLUT4 in L6 myotubes treated with YPG (0.1 μM, 0.5 h) or YPP (0.1 μM, 0.5 h) were measured by the WES analysis to evaluate the effect of the tripeptides on GLUT4 translocation in L6 myotubes. Results are displayed as virtual blot-like images and electropherograms. Results are presented as mean ± SEM (n = 4). Statistical differences were assessed by Tukey-Kramer test. Means with different letters represent statistically different at $p < 0.05$.

3.5. Determination of tripeptides in soybean hydrolysate by LC-TOF/MS analysis

Using a LC-TOF/MS-aided standard addition method,[96] the determination of YPG and YPP in a commercially soybean hydrolysate. According to the standard addition curve between the amount of spiked YPP and MS signal intensity (y = 10093x + 300692, r^2 = 0.999), the amount of YPP in the soybean hydrolysate was successfully quantified to be 29.8 μg/g-hydrolysate (Figs. 3-9B and C). Whereas no detection of YPG was confirmed in the soybean hydrolysate (Fig. 3-9A). These findings suggest that the AdipoR1 agonistic tripeptide YPP may be produced by the enzymatic hydrolysis of soybean proteins, according to the sequence prediction listed in Table 3-1. Based on the observation that the soybean hydrolysate contains 29.8 μg/g YPP and 470 μg/g YP[56], it was shown that YPP is a naturally occurring tripeptide with notable AdipoR1 agonistic activity. In addition, considering that Pro-containing peptides have a relatively higher resistance against protease degradation,[59] a higher bioavailability of YPP (and YP as well) in the bloodstream would be expected. However, further animal studies on their bioavailability including absorption and tissue accumulation are required.

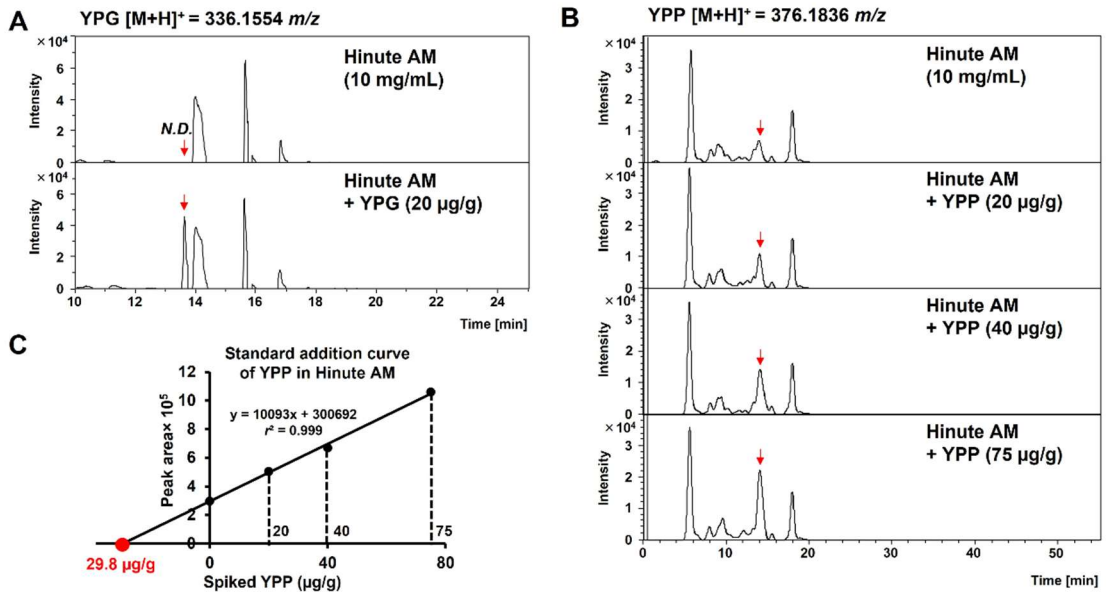

Fig. 3-9. Quantitative detection of tripeptides in soybean hydrolysate by LC-TOF/MS analysis.

Extracted ion-chromatograms of YPG (336.1554 *m/z*) (A) and YPP (376.1836 *m/z*) (B) in soybean hydrolysate (10 mg/mL) and the hydrolysate spiked with YPG (20 μg/g) or YPP (20, 40, and 75 μg/g) were acquired. According to the standard addition curve of YPP in the soybean hydrolysate (y = 10093x + 300692, r^2 = 0.999), the amount of YPP was calculated in the hydrolysate at 29.8 μg/g (C). *N.D.* = no detection.

3.6. *In silico* MD simulation analysis of tripeptide-AdipoR1 docking complexes

In silico MD simulation analysis was performed to gain insight into the structural requirements of active tripeptides, such as YPG and YPP, for AdipoR1 agonistic activity. Tripeptides of YPG and YPP were virtually docked with AdipoR1, and their complexes were simulated in POPC membrane for 200 ns. The virtually constructed complexes of YPG and YPP with site 1 (Fig. 3-10A) and site 2 (Fig. 3-11A) of AdipoR1 embedded in the POPC membrane showed a stable MD trajectory with an RMSD value of < 5.0 Å during 180–200 ns of the simulation. The stable simulations for both tripeptides also provided information on the intermolecular interaction between the tripeptides and sites 1/2 of AdipoR1 in the POPC membrane (Figs. 3-10B and 3-11B). The ΔG_{bind} values (Fig. 3-10B) suggested that the binding potency of YPG and YPP to site 1 of AdipoR1 was comparable with that of YP, although AdipoRon had a higher ΔG_{bind} value. The higher ΔG_{bind} of YPP compared to those of YP and YPG at site 2 (Fig. 3-11B) and YPP at site 1 (Fig. 3-10B) suggests that YPP may preferentially bind to site 2 of AdipoR1. From the results of the per-residue decomposition analysis, six residues (Trp^{223}, Gly^{275}, Leu^{276}, Gln^{299}, Phe^{303}, and His^{351}) and seventeen residues (Ile^{216}, Ser^{219}, Phe^{220}; Trp^{223}, Arg^{267}, Gly^{275}, Leu^{276}, Gly^{278}, Val^{279}, Thr^{282}, Glu^{289}, Gln^{299}, Tyr^{310}, Arg^{320}, His^{351}, Glu^{360}, and Glu^{366}) at site 1 of AdipoR1 were found to be involved in the binding of YPG and YPP, respectively (Figs. 3-10B and C). At site 2 of AdipoR1, eight residues (Phe^{148},

Arg^{158}, Glu^{169}, Leu^{215}, Gly^{218}, Ser^{219}, Arg^{267}, and Ala^{348}) and nine residues (Arg^{158}, Asn^{160}, Lys^{170}, Phe^{173}, His^{351}, Phe^{352}, Ser^{356}, Gln^{359}, and Glu^{360}) were observed to be involved in the binding of YPG and YPP, respectively (Figs. 3-11B and C). In particular, His^{351} at site 1 and Arg^{158} at site 2 are common amino acid residues involved in binding the four AdipoR1 agonists (AdipoRon, YP, YPG, and YPP), suggesting their key role in the seven-transmembrane AdipoR1 for ligand binding.

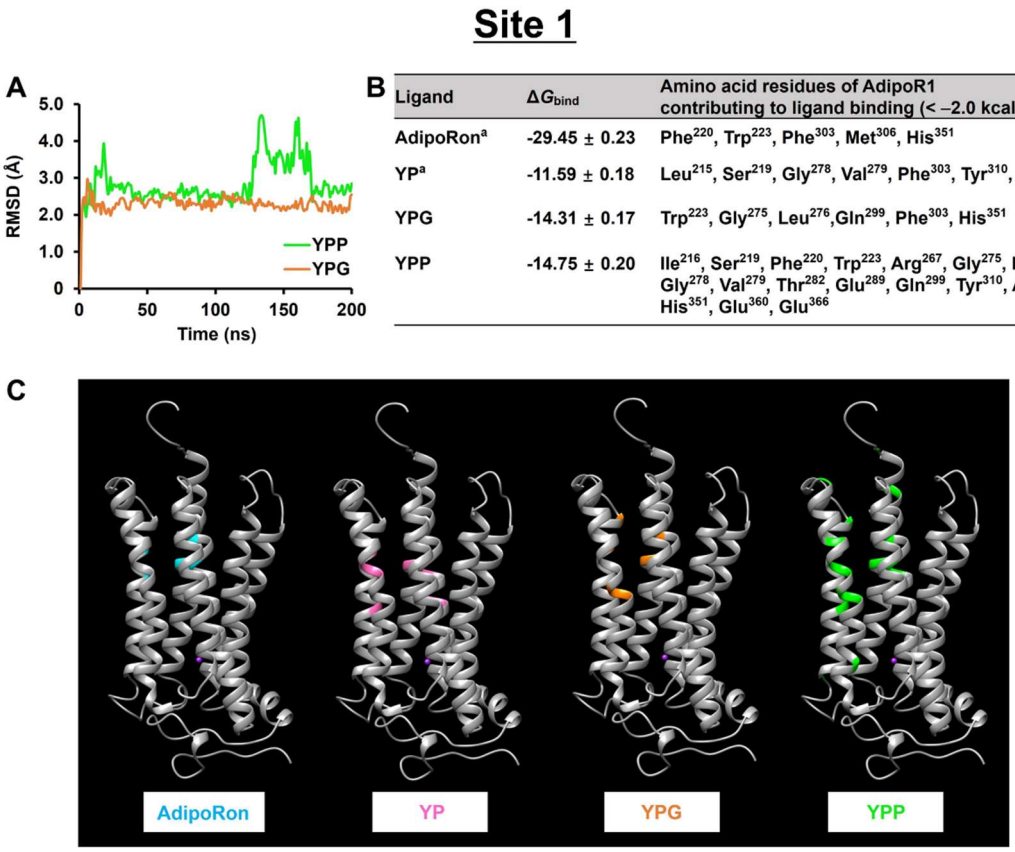

Fig. 3-10. MD simulation analyses of YPG- and YPP-AdipoR1-POPC complexes at site 1 of AdipoR1.

Protein backbone root-mean-square deviation (RMSD) values from the initial structure of the ligand-AdipoR1-POPC complexes were computed for 200 ns (A). The Gibbs free energy of binding values, ΔG_{bind} (kcal/mol) of the ligand-AdipoR1 complexes in POPC were estimated for 180–200 ns (B). Each amino acid residue that contributed to < -2.0 kcal/mol binding at site 1 of AdipoR1 (B) were visualized in the following colors: AdipoRon, blue; YP, pink; YPG, orange; YPP, green (C). Superscript (a) is the result described in **Chapter II**.

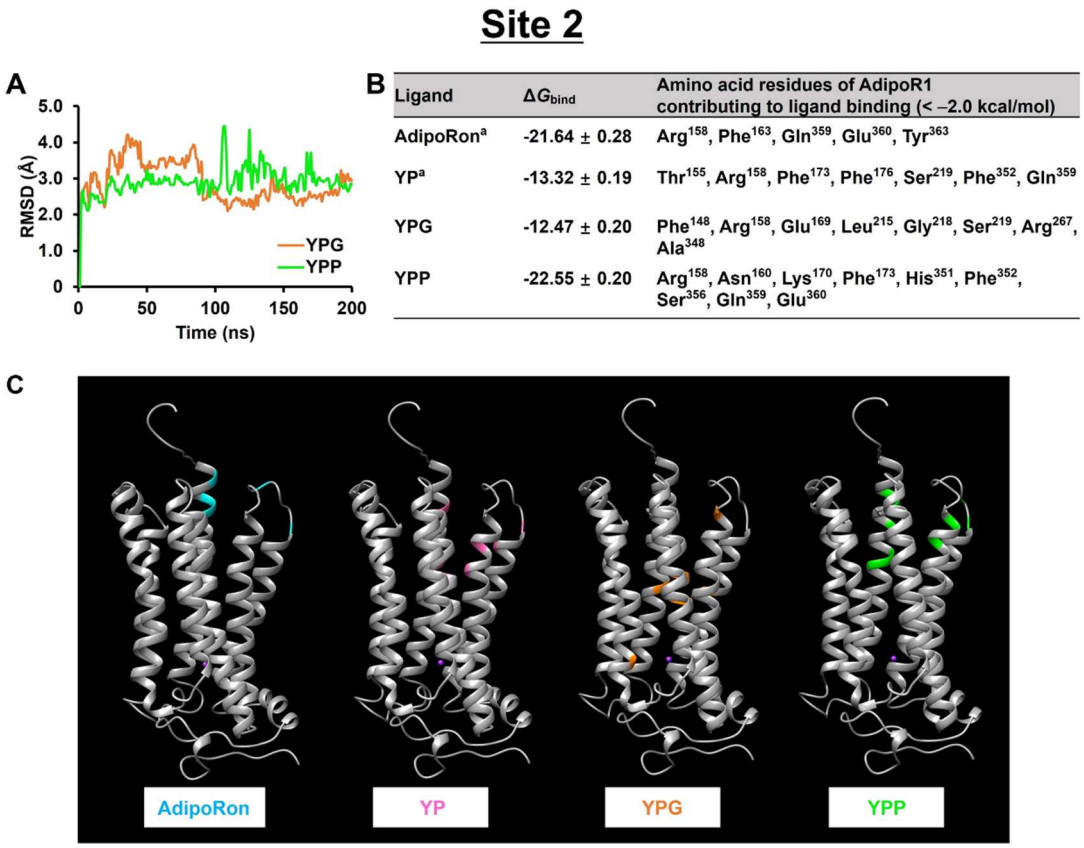

Fig. 3-11. MD simulation analyses of YPG- and YPP-AdipoR1-POPC complexes at site 2 of AdipoR1.

Protein backbone root-mean-square deviation (RMSD) values from the initial structure of the ligand-AdipoR1-POPC complexes were computed for 200 ns (A). The Gibbs free energy of binding values, ΔG_{bind} (kcal/mol) of the ligand-AdipoR1 complexes in POPC were estimated for 180–200 ns (B). Each amino acid residue that contributed to < -2.0 kcal/mol binding at site 2 of AdipoR1 (B) were visualized in the following colors: AdipoRon, blue; YP, pink; YPG, orange; YPP, green (C). Superscript (a) is the result described in **Chapter II**.

The *in silico* observations obtained in this study agreed with Ma *et al*.,[40] who simulated a virtual complex of a heptapeptide, PGLYYFD, with AdipoR1 via hydrogen bonding of PGLYYFD with Arg^{158} of AdipoR1, together with Gln^{359} and Tyr^{353}. It was also revealed that Tyr at the N-terminus and Pro at the C-terminus in the skeletons of YPG (Fig. 3-12) and YPP (Fig. 3-13) contributed to its stable binding to AdipoR1 via intermolecular interactions, including hydrogen, hydrophobic, and π–π electron bonds. These observations indicate that oligo- (> tetra-) peptides with aromatic amino acids and/or amino acids capable of interacting with His and Arg at both N- and C-termini may be essential for notable AdipoR1 agonistic effect.

Site 1

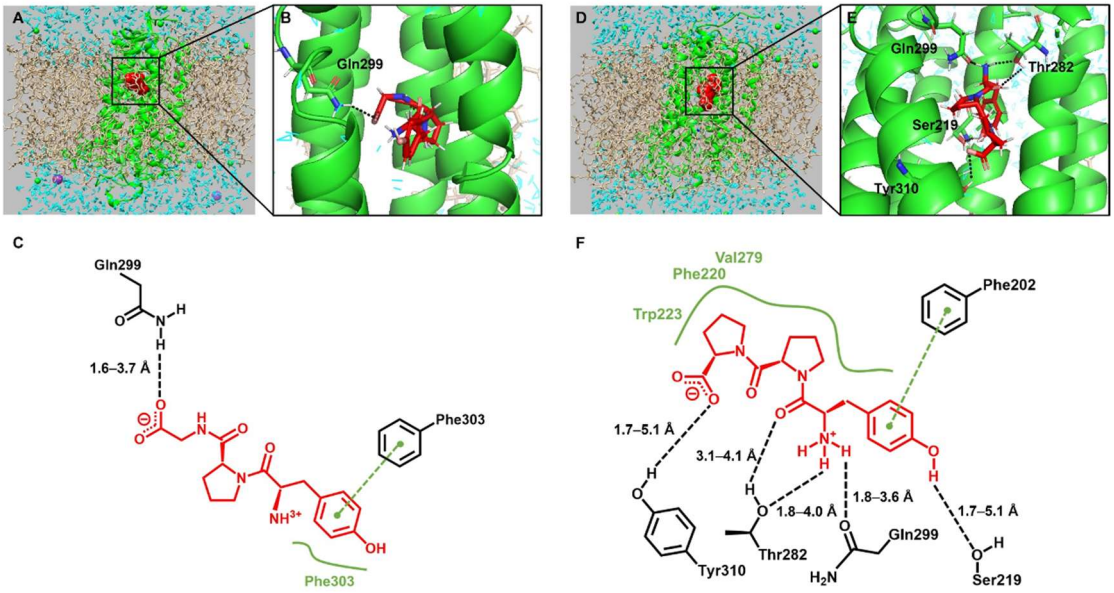
A
B
Gln299
D
E
Gln299
Thr282
Ser219
Tyr310
C
Gln299
1.6–3.7 Å
Phe303
NH3+
OH
Phe303
F
Val279
Phe220
Trp223
Phe202
1.7–5.1 Å
3.1–4.1 Å
1.8–3.6 Å
1.8–4.0 Å
1.7–5.1 Å
Thr282
Gln299
Tyr310
H2N
Ser219

Site 2

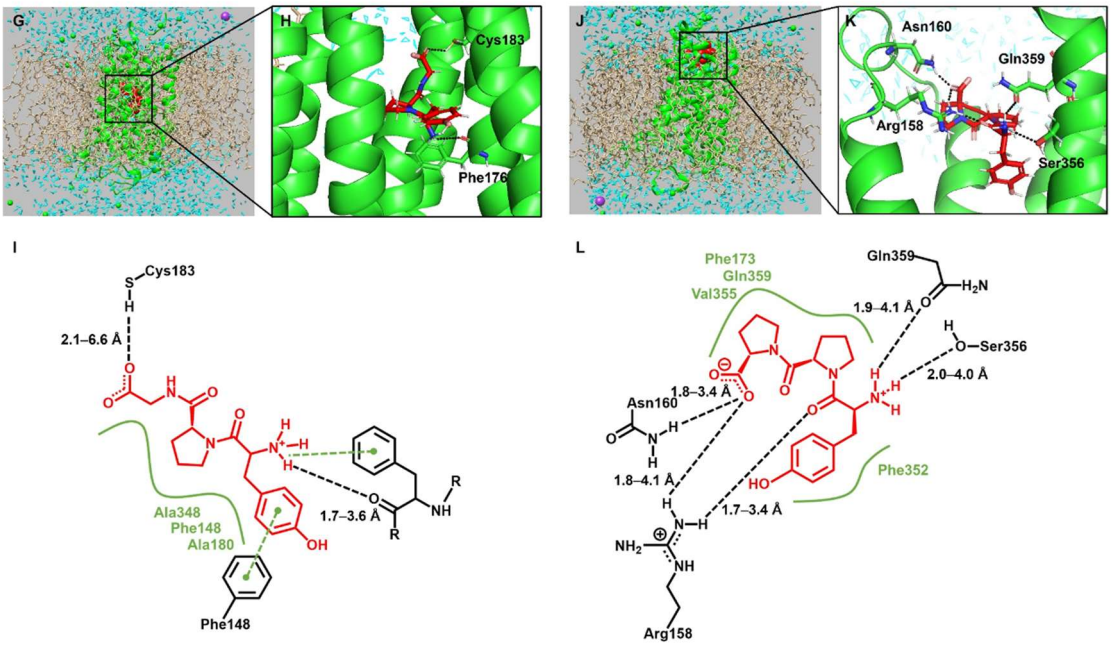
G
H
Cys183
Phe176
J
K
Asn160
Gln359
Arg158
Ser356
I
Cys183
2.1–6.6 Å
1.7–3.6 Å
Ala348
Phe148
Ala180
OH
Phe148
L
Phe173
Gln359
Val355
Gln359
1.9–4.1 Å
Ser356
2.0–4.0 Å
1.8–3.4 Å
Asn160
1.8–4.1 Å
1.7–3.4 Å
Phe352
NH2
NH
Arg158

Fig. 3-12. *In silico* MD simulation analysis at sites 1/2.

MD simulation analyses of the CHARMM-GUI-aided YPG-AdipoR1-POPC complex (A) and YPP-AdipoR1-POPC complex (D) at site 1 (ligand, red; AdipoR1, green; Na^+, green sphere; Cl^-, purple sphere; POPC, brown; water molecule, cyan). Binding conformations of YPG (B; T = 182 ns) and YPP complexes (E; T = 198 ns) were visualized (C atom, red; H atom, white; N atom, blue; O atom, pink). Intermolecular interactions of YPG (C; T = 182 ns) and YPP complexes (F; T = 198 ns) were visualized (hydrogen bond, black dashed line; hydrophobic interaction, green straight line; π–π electron interaction, green dashed line).

MD simulation analyses of the CHARMM-GUI-aided YPG-AdipoR1-POPC complex (G) and YPP-AdipoR1-POPC complex (J) at site 2 (ligand, red; AdipoR1, green; Na^+, green sphere; Cl^-, purple sphere; POPC, brown; water molecule, cyan). Binding conformations of YPG (H; T = 190 ns) and YPP complexes (K; T = 181 ns) were visualized (C atom, red; H atom, white; N atom, blue; O atom, pink). Intermolecular interactions of YPG (I; T = 190 ns) and YPP complexes (L; T = 181 ns) were visualized (hydrogen bond, black dashed line; hydrophobic interaction, green straight line; π–π electron interaction, green dashed line).

4. Summary

In **Chapter III**, the results from *in vitro* L6 cell and *in silico* MD simulation experiments demonstrated that the tripeptides YPG and YPP are notable AdipoR1 agonists, comparable to the synthetic drug, AdipoRon. The finding that YPP (glycinin G5 295–297) is present in soybean hydrolysate at 29.8 μg/g together with the reported AdipoR1 agonistic dipeptide YP (470 μg/g)[56] strongly implies that the soybean hydrolysate can be a useful alternative anti-diabetic food material, with its mechanism of action involving adiponectin-like glucose uptake in muscles.

Chapter IV

Conclusion

The incidence of insulin-independent type 2 diabetes mellitus (T2DM), characterized by insulin resistance and hyperglycemia, and its related complications continues to increase worldwide.[3] Although glucose uptake mostly takes place in skeletal muscle in the postprandial period,[70] considerable evidence indicates that adiponectin is also involved in regulating glucose uptake by activating adenosine monophosphate-activated protein kinase (AMPK) in a manner distinct from that of insulin signaling.[28] Adiponectin is an adipocyte-derived hormone that acts via two adiponectin receptor 1/2 (AdipoR1/2). AdipoR1 is ubiquitously expressed and is mainly abundant in skeletal muscle, whereas AdipoR2 expression is mainly restricted to the liver.[25] The adiponectin intracellular signaling for glucose uptake by skeletal muscle primarily includes the AdipoR1-medaited AMPK/glucose transporter 4 (GLUT4) translocation pathway.[32-33] Thus, targeted stimulation of the adiponectin signaling pathway or the development of skeletal muscle AdipoR1 agonists may be an effective

strategy for preventing and managing insulin-independent T2DM. However, adiponectin-like drugs are not currently available as direct therapeutics, except for the small drug, AdipoRon[42] because of the difficulties in converting full-size adiponectin (244-amino acids) into a viable agent. Therefore, the goal of the present study was to investigate AdipoR1-agonsitic di- (**Chapter II**) and tripeptides (**Chapter III**) rather than longer oligopeptides using *in vitro* L6 cells and *in silico* molecular dynamics (MD) simulation analyses because of their favorable absorption.

Chapter II Adiponectin receptor agonistic action of dipeptides by *in vitro* rat skeletal muscle L6 cells and *in silico* analyses

The aim of this study was to develop dipeptides showing an AdipoR1 agonistic action in skeletal muscle. Fifteen dipeptides with the structural similarity to a synthetic AdipoR agonist, AdipoRon, were targeted for glucose uptake experiments in rat skeletal muscle L6 cells. Among the dipeptides, Tyr-Pro (YP) showed a significant promotion of glucose uptake, while other dipeptides, including Pro-Tyr (PY), failed to exert the effect. YP significantly induced GLUT4 translocation to the plasma membrane, along with AMPK activation. By knockdown of AdipoR1 expression, the increased glucose uptake by YP was abolished, indicating that YP may play a promoting role in the glucose uptake through the AdipoR1-mediated AMPK/GLUT4 translocation pathway in L6 cells. The preferable MD simulation of YP toward the AdipoR1 was also

confirmed by the CHARMM-GUI-aided *in silico* analysis, in which YP was stably positioned in the two potential binding sites 1/2 of AdipoR1 embedded in a virtual phospholipid membrane. Consequently, these findings demonstrate the anti-diabetic function of the dipeptide YP, present in soybean hydrolysate, as a possible AdipoR1 agonist.

Chapter III Adiponectin receptor agonistic action of soybean tripeptides by *in vitro* skeletal muscle L6 cells and *in silico* analyses

In **Chapter II**, it was demonstrated that dipeptide YP can serve as an AdipoR1 agonist. According to the dipeptide YP study, further experiments were performed to investigate the AdipoR1-agonistic potential of YP-related tripeptides by *in vitro* L6 cells and *in silico* MD simulation analyses. Seventeen YP-related tripeptides in the sequence of soybean proteins were synthesized and subjected to glucose uptake experiment in rat skeletal muscle L6 cells. Among the tripeptides, those elongated at the C-terminal of YP, Tyr-Pro-Gly (YPG), Tyr-Pro-Glu (YPE), Tyr-Pro-Pro (YPP), and Tyr-Pro-Gln (YPQ), significantly promoted glucose uptake in L6 cells, similar to the effect of AdipoRon. Knockdown of AdipoR1 expression in L6 cells abrogated this effect of YPG and YPP, indicating that the two tripeptides had an AdipoR1 agonistic action. Moreover, the CHARMM-GUI-aided MD simulation in a virtual phospholipid membrane revealed that YPG and YPP were stably positioned in the two potential binding sites 1/2 of AdipoR1 (ΔG_{bind} < -10 kcal/mol). Consequently,

these findings demonstrate that the soybean tripeptides YPG and YPP, with AdipoR1 agonistic YP sequence, have alternative adiponectin-like potential via their preferential binding to AdipoR1.

Taken together all, the present study demonstrates for the first time that these small di-/tripeptides may be alternative-medicinal food compounds against insulin-independent T2DM, with their mechanism of action involving adiponectin-like glucose uptake in skeletal muscle.

References

[1] Sun, H.; Saeedi, P.; Karuranga, S.; Pinkepank, M.; Ogurtsova, K.; Duncan, B. B.; Magliano, D. J. IDF Diabetes Atlas: Global, regional and country-level diabetes prevalence estimates for 2021 and projections for 2045. *Diabetes Res. Clin. Pract.* **2022**, *183*, 109119.

[2] Saeedi, P.; Petersohn, I.; Salpea, P.; Malanda, B.; Karuranga, S.; Unwin, N.; Committee, I. D. A. Global and regional diabetes prevalence estimates for 2019 and projections for 2030 and 2045: Results from the International Diabetes Federation Diabetes Atlas. *Diabetes Res. Clin. Pract.* **2019**, *157*, 107843.

[3] Khan, M. A. B.; Hashim, M. J.; King, J. K.; Govender, R. D.; Mustafa, H.; Al Kaabi, J. Epidemiology of type 2 diabetes–global burden of disease and forecasted trends. *J. Epidemiol. Glob. Health* **2020**, *10*, 107–111.

[4] Prentki, M.; Nolan, C. J. Islet β cell failure in type 2 diabetes. *J. Clin. Investig.* **2006**, *116*, 1802–1812.

[5] Forbes, J. M.; Cooper, M. E. Mechanisms of diabetic complications. *Physiol. Rev.* **2013**, *93*, 137–188.

[6] Scherer, P. E.; Williams, S.; Fogliano, M.; Baldini, G.; Lodish, H. F. A novel serum protein similar to C1q, produced exclusively in adipocytes. *J. Biol. Chem.* **1995**, *270*, 26746–26749.

[7] Hu, E.; Liang, P.; Spiegelman, B. M. AdipoQ is a movel adipose-specific gene dysregulated in obesity. *J. Biol. Chem.* **1996**, *271*, 10697–10703.

[8] Maeda, K.; Okubo, K.; Shimomura, I.; Funahashi, T.; Matsuzawa, Y.; Matsubara, K. cDNA cloning and expression of a novel adipose specific collagen-like factor, apM1 (AdiPoseMost abundant Gene transcript 1). *Biochem. Biophys. Res. Commun.* **1996**, *221*, 286–289.

[9] Nakano, Y.; Tobe, T.; Choi-Miura, N. H.; Mazda, T.; Tomita, M. Isolation and characterization of GBP28, a novel gelatin-binding protein purified from human plasm. *J. Biochem.* **1996**, *120*, 803–812.

[10] Mojiminiyi, O. A.; Abdella, N. A.; Al Arouj, M.; Ben Nakhi, A. Adiponectin, insulin resistance and clinical expression of the metabolic syndrome in patients with Type 2 diabetes. *Int. J. Obes. (Lond.)* **2007**, *31*, 213–220.

[11] Abdella, N. A.; Mojiminiyi, O. A. Clinical applications of adiponectin measurements in type 2 diabetes mellitus: screening, diagnosis, and marker of diabetes control. *Dis. Markers* **2018**, 5187940.

[12] Kelesidis, I.; Kelesidis, T.; Mantzoros, C. Adiponectin and cancer: a systematic review. *Br. J. Cancer* **2006**, *94*, 1221–1225.

[13] Ouchi, N.; Walsh, K. Adiponectin as an anti-inflammatory factor. *Clin. Chim. Acta* **2007**, *380*, 24–30.

[14] Han, S. H.; Quon, M. J.; Kim, J. A.; Koh, K. K. Adiponectin and cardiovascular disease: response to therapeutic interventions. *J. Am. Coll. Cardiol.* **2007**, *49*, 531–538.

[15] Berg, A. H.; Combs, T. P.; Scherer, P. E. ACRP30/adiponectin: an adipokine regulating glucose and lipid metabolism. *Trends Endocrinol. Metab.* **2002**, *13*, 84–89.

[16] Schraw, T.; Wang, Z. V.; Halberg, N.; Hawkins, M.; Scherer, P. E. Plasma adiponectin complexes have distinct biochemical characteristics. *Endocrinology* **2008**, *149*, 2270–2282.

[17] Swarbrick, M. M.; Havel, P. J. Physiological, pharmacological, and nutritional regulation of circulating adiponectin concentrations in humans. *Metab. Syndr. Relat. Disord.* **2008**, *6*, 87–102.

[18] Chandran, M.; Phillips, S. A.; Ciaraldi, T.; Henry, R. R. Adiponectin: more than just another fat cell hormone? *Diabetes Care* **2003**, *26*, 2442–2450.

[19] Yamauchi, T.; Kamon, J.; Waki, H.; Terauchi, Y.; Kubota, N.; Hara, K.; Mory, Y.; Ide, T.; Murakami, K.; Tsuboyama-Kasaoka, N.; Ezaki, O.; Akanuma, Y.; Gavrilova, O.; Vinson, C.; Reitman, M. L.; Kagechika, H.; Shudo, K.; Yoda, M.; Nakano, Y.; Tobe, K.; Nagai, R.; Kimura, S.; Tomita, M.; Froguel, P.; Kadowaki, T. The fat-derived hormone adiponectin reverses insulin resistance associated with both lipoatrophy and obesity. *Nat. Med.* **2001**, *7*, 941–946.

[20] Antonopoulos, A. S.; Margaritis, M.; Coutinho, P.; Shirodaria, C.; Psarros, C.; Herdman, L.; Antoniades, C. Adiponectin as a link between type 2 diabetes and vascular NADPH oxidase activity in the human arterial wall: the regulatory role of perivascular adipose tissue. *Diabetes*

2015, *64*, 2207–2219.

[21] Berg, A. H.; Combs, T. P.; Du, X.; Brownlee, M.; Scherer, P. E. The adipocyte-secreted protein Acrp30 enhances hepatic insulin action. *Nat. Med.* **2001**, *7*, 947–953.

[22] Fruebis, J.; Tsao, T. S.; Javorschi, S.; Ebbets-Reed, D.; Erickson, M. R. S.; Yen, F. T.; Bihain, B. E.; Lodish, H. F. Proteolytic cleavage product of 30-kDa adipocyte complement-related protein increases fatty acid oxidation in muscle and causes weight loss in mice. *Proc. Natl. Acad. Sci. U.S.A.* **2001**, *98*, 2005–2010.

[23] Combs, T. P.; Pajvani, U. B.; Berg, A. H.; Lin, Y.; Jelicks, L. A.; Laplante, M.; Nawrocki, A. R.; Rajala, M. W.; Parlow, A. F.; Cheeseboro, L.; Ding, Y. Y.; Russell, R. G.; Lindemann, D.; Hartley, A.; Baker, G. R. C.; Obici, S.; Deshaies, Y.; Ludgate, M.; Rossetti, L.; Scherer, P. E. A transgenic mouse with a deletion in the collagenous domain of adiponectin displays elevated circulating adiponectin and improved insulin sensitivity. *Endocrinology* **2004**, *145*, 367–383.

[24] Maeda, N.; Shimomura, I.; Kishida, K.; Nishizawa, H.; Matsuda, M.; Nagaretani, H.; Furuyama, N.; Kondo, H.; Takahashi, M.; Arita, Y.; Komuro, R.; Ouchi, N.; Kihara, S.; Tochino, Y.; Okutomi, K.; Horie, M.; Takeda, S.; Aoyama, T.; Funahashi, T.; Matsuzawa, Y. Diet-induced insulin resistance in mice lacking adiponectin/ACRP30. *Nat. Med.* **2002**, *8*, 731–737.

[25] Yamauchi, T.; Kamon, J.; Ito, Y.; Tsuchida, A.; Yokomizo, T.; Kita, S.;

Sugiyama, T.; Miyagishi, M.; Hara, K.; Tsunoda, M.; Murakami, K.; Ohteki, T.; Uchida, S.; Takekawa, S.; Waki, H.; Tsuno, N. H.; Shibata, Y.; Terauchi, Y.; Froguel, P.; Tobe, K., et al. Cloning of adiponectin receptors that mediate antidiabetic metabolic effects. *Nature* **2003**, *423*, 762–769.

[26] Kadowaki, T.; Yamauchi, T. Adiponectin and adiponectin receptors. *Endocr. Rev.* **2005**, *26*, 439–451.

[27] Mao, X.; Kikani, C. K.; Riojas, R. A.; Langlais, P.; Wang, L.; Ramos, F. J.; Fang, Q.; Christ-Roberts, C. Y.; Hong, J. Y.; Kim, R. Y.; Liu, F.; Dong, L. Q. APPL1 binds to adiponectin receptors and mediates adiponectin signalling and function. *Nat. Cell Biol.* **2006**, *8*, 516–523.

[28] Yamauchi, T.; Kamon, J.; Minokoshi, Y.; Ito, Y.; Waki, H.; Uchida, S.; Yamashita, S.; Noda, M.; Kita, S.; Ueki, K.; Eto, K.; Akanuma, Y.; Froguel, P.; Foufelle, F.; Ferre, P.; Carling, D.; Kimura, S.; Nagai, R.; Kahn, B. B.; Kadowaki, T. Adiponectin stimulates glucose utilization and fatty-acid oxidation by activating AMP-activated protein kinase. *Nat. Med.* **2002**, *8*, 1288–1295.

[29] Viollet, B.; Foretz, M.; Guigas, B.; Horman, S.; Dentin, R.; Bertrand, L.; Hue, L.; Andreelli, F. Activation of AMP-activated protein kinase in the liver: a new strategy for the management of metabolic hepatic disorders. *J. Physiol. Paris* **2006**, *574*, 41–53.

[30] Sanz, P. AMP-activated protein kinase: structure and regulation. *Curr. Protein Pept. Sci.* **2008**, *9*, 478–492.

[31] Fullerton, M. D.; Galic, S.; Marcinko, K.; Sikkema, S.; Pulinilkunnil, T.;

Chen, Z. P.; O'Neill, H. M.; Ford, R. J.; Palanivel, R.; O'Brien, M.; Hardie, D. G.; Macaulay, S. L.; Schertzer, J. D.; Dyck, J. R. B.; Denderen, B. J. V.; Van, B. J.; Kemp, B. E.; Steinberg, G. R. Single phosphorylation sites in Acc1 and Acc2 regulate lipid homeostasis and the insulin-sensitizing effects of metformin. *Nat. Med.* **2013**, *19*, 1649–1654.

[32] Ceddia, R. B.; Somwar, R.; Maida, A.; Fang, X.; Bikopoulos, G.; Sweeney, G. Globular adiponectin increases GLUT4 translocation and glucose uptake but reduces glycogen synthesis in rat skeletal muscle cells. *Diabetologia* **2005**, *48*, 132–139.

[33] Vu, V.; Bui, P.; Eguchi, M.; Xu, A.; Sweeney, G. Globular adiponectin induces LKB1/AMPK-dependent glucose uptake via actin cytoskeleton remodeling. *J. Mol. Endocrinol.* **2013**, *51*, 155–165.

[34] Civitarese, A. E.; Ukropcova, B.; Carling, S.; Hulver, M.; DeFronzo, R. A.; Mandarino, L.; Ravussin, E.; Smith, S. R. Role of adiponectin in human skeletal muscle bioenergetics. *Cell Metab.* **2006**, *4*, 75–87.

[35] Andreelli, F.; Foretz, M.; Knauf, C.; Cani, P. D.; Perrin, C.; Iglesias, M. A.; Pillot, B.; Bado, A.; Tronche, F.; Mithieux, G.; Vaulont, S.; Burcelin, R.; Viollet, B. Liver adenosine monophosphate-activated kinase-α2 catalytic subunit is a key target for the control of hepatic glucose production by adiponectin and leptin but not insulin. *Endocrinology* **2006**, *147*, 2432–2441.

[36] Otvos Jr, L. Potential adiponectin receptor response modifier therapeutics. *Front. Endocrinol.* **2019**, *10*, 539.

[37] Hossain, M. M.; Mukheem, A.; Kamarul, T. The prevention and treatment of hypoadiponectinemia-associated human diseases by up-regulation of plasma adiponectin. *Life Sci.* **2015**, *135*, 55–67.

[38] Otvos, L.; Haspinger, E.; La Russa, F.; Maspero, F.; Graziano, P.; Kovalszky, I.; Cassone, M. Design and development of a peptide-based adiponectin receptor agonist for cancer treatment. *BMC Biotechnol.* **2011**, *11*, 90.

[39] Sayeed, M.; Gautam, S.; Verma, D. P.; Afshan, T.; Kumari, T.; Srivastava, A. K.; Ghosh, J. K. A collagen domain–derived short adiponectin peptide activates APPL1 and AMPK signaling pathways and improves glucose and fatty acid metabolisms. *J. Biol. Chem.* **2018**, *293*, 13509–13523.

[40] Ma, L.; Zhang, Z.; Xue, X.; Wan, Y.; Ye, B.; Lin, K. A potent peptide as adiponectin receptor 1 agonist to against fibrosis. *J. Enzyme Inhib. Med. Chem.* **2017**, *32*, 624–631.

[41] Kim, S.; Lee, Y.; Kim, J. W.; Son, Y. J.; Ma, M. J.; Um, J. H.; Kim, N. D.; Min, S. H.; Kim, D. I.; Kim, B. B. Discovery of a novel potent peptide agonist to adiponectin receptor 1. *PLoS One* **2018**, *13*, e0199256.

[42] Okada-Iwabu, M.; Yamauchi, T.; Iwabu, M.; Honma, T.; Hamagami, K.; Matsuda, K.; Yamaguchi, M.; Tanabe, H.; Kimura-Someya, T.; Shirouzu, M.; Ogata, H.; Tokuyama, K.; Ueki, K.; Nagano, T.; Tanaka, A.; Yokoyama, S.; Kadowaki, T. A small-molecule AdipoR agonist for type 2 diabetes and short life in obesity. *Nature* **2013**, *503*, 493–499.

[43] Zhang, Y.; Zhao, J.; Li, R.; Lau, W. B.; Yuan, Y. X.; Liang, B.; Li, R.;

Gao, E. H.; Koch, W. J.; Ma, X. L.; Wang, Y. J. AdipoRon, the first orally active adiponectin receptor activator, attenuates postischemic myocardial apoptosis through both AMPK-mediated and AMPK-independent signalings. *Am. J. Physiol. - Endocrinol. Metab.* **2015**, *309*, E275–E282.

[44] Ramzan, A. A.; Bitler, B. G.; Hicks, D.; Barner, K.; Qamar, L.; Behbakht, K.; Powell, T.; Jansson, T.; Wilson, H. Adiponectin receptor agonist AdipoRon induces apoptotic cell death and suppresses proliferation in human ovarian cancer cells. *Mol. Cell. Biochem.* **2019**, *461*, 37–46.

[45] Nicolas, S.; Debayle, D.; Béchade, C.; Maroteaux, L.; Gay, A. S.; Bayer, P.; Heurteaux, C.; Guyon, A.; Chabry, J. Adiporon, an adiponectin receptor agonist acts as an antidepressant and metabolic regulator in a mouse model of depression. *Transl. Psychiatry* **2018**, *8*, 1–11.

[46] Wang, Y.; Wan, Y.; Ye, G.; Wang, P.; Xue, X.; Wu, G.; Ye, B. Hepatoprotective effects of AdipoRon against d-galactosamine-induced liver injury in mice. *Eur. J. Pharm. Sci* . **2016**, *93*, 123–131.

[47] Zheng, J.; Sun, Z.; Liang, F.; Xu, W.; Lu, J.; Shi, L.; Shao, A.; Yu, J.; Zhang, J. AdipoRon attenuates neuroinflammation after intracerebral hemorrhage through AdipoR1-AMPK pathway. *Neuroscience* **2019**, *412*.

[48] Mine, Y.; Matsui, T. Current understanding of bioaccessibility and bioavailability of food-derived bioactive peptides. *Int. J. Food Sci. Technol.* **2019**, *54*, 2319–2320.

[49] Korhonen, H.; Pihlanto, A. Food-derived bioactive peptides-opportunities for designing future foods. *Curr. Pharm. Des.* **2003**, *9*,

1297–1308.

[50] Xu, Q.; Yan, X.; Zhang, Y.; Wu, J. Current understanding of transport and bioavailability of bioactive peptides derived from dairy proteins: a review. *Int. J. Food Sci.* **2019**, *54*, 1930–1941.

[51] Miner-Williams, W. M.; Stevens, B. R.; Moughan, P. J. Are intact peptides absorbed from the healthy gut in the adult human? *Nutr. Res. Rev.* **2014**, *27*, 308–329.

[52] Matsui, T.; Sato, M.; Tanaka, M.; Yamada, Y.; Watanabe, S.; Fujimoto, Y.; Imaizumi, K.; Matsumoto, K. Vasodilating dipeptide Trp-His can prevent atherosclerosis in apo E-deficient mice. *Br. J. Nutr.* **2010**, *103*, 309–313.

[53] Matsui, T.; Tamaya, K.; Seki, E.; Osajima, K.; Matsumoto, K.; Kawasaki, T. Val-Tyr as a natural antihypertensive dipeptide can be absorbed into the human circulatory blood system. *Clin. Exp. Pharmacol. Physiol.* **2002**, *29*, 204–208.

[54] Tanaka, M.; Hong, S. M.; Akiyama, S.; Hu, Q. Q.; Matsui, T. Visualized absorption of anti-atherosclerotic dipeptide, Trp-His, in Sprague–Dawley rats by LC-MS and MALDI-MS imaging analyses. *Mol. Nutr. Food Res.* **2015**, *59*, 1541–1549.

[55] Hong, S. M.; Tanaka, M.; Yoshii, S.; Mine, Y.; Matsui, T. Enhanced visualization of small peptides absorbed in rat small intestine by phytic-acid-aided matrix-assisted laser desorption/ionization-imaging mass spectrometry. *Anal. Chem.* **2013**, *85*, 10033–10039.

[56] Tanaka, M.; Dohgu, S.; Komabayashi, G.; Kiyohara, H.; Takata, F.; Kataoka, Y.; Nirasawa, T.; Maebuchi, M.; Matsui, T. Brain-transportable dipeptides across the blood-brain barrier in mice. *Sci. Rep.* **2019**, *9*, 1–10.

[57] Tanaka, M.; Kiyohara, H.; Yoshino, A.; Nakano, A.; Takata, F.; Dohgu, S.; Kataoka, Y.; Matsui, T. Brain-transportable soy dipeptide, Tyr-Pro, attenuates amyloid β peptide25-35-induced memory impairment in mice. *npj Sci. Food.* **2020**, *4*, 1–4.

[58] Nakamura, Y.; Yamamoto, N.; Sakai, K.; Takano, T. Antihypertensive effect of sour milk and peptides isolated from it that are inhibitors to angiotensin I-converting enzyme. *Int. J. Dairy Sci.* **1995**, *78*, 1253–1257.

[59] Vanhoof, G.; Goossens, F.; De Meester, I.; Hendriks, D.; Scharpé, S. Proline motifs in peptides and their biological processing. *FASEB J.* **1995**, *9*, 736–744.

[60] Soga, M.; Ohashi, A.; Taniguchi, M.; Matsui, T.; Tsuda, T. The di-peptide Trp-His activates AMP-activated protein kinase and enhances glucose uptake independently of insulin in L6 myotubes. *FEBS Open Bio* **2014**, *4*, 898–904.

[61] Kobayashi, Y.; Kovacs-Nolan, J.; Matsui, T.; Mine, Y. The anti-atherosclerotic dipeptide, Trp-His, reduces intestinal inflammation through the blockade of L-type Ca^{2+} channels. *J. Agric. Food Chem.* **2015**, *63*, 6041–6050.

[62] Matsui, T.; Ueno, T.; Tanaka, M.; Oka, H.; Miyamoto, T.; Osajima, K.;

Matsumoto, K. Antiproliferative action of an angiotensin I-converting enzyme inhibitory peptide, Val-Tyr, via an $_{L}$-type Ca^{2+} channel inhibition in cultured vascular smooth muscle cells. *Hypertens. Res.* **2005**, *28*, 545–552.

[63] Okamoto, K.; Kawamura, S.; Tagawa, M.; Mizuta, T.; Zahid, H. M.; Nabika, T. Production of an antihypertensive peptide from milk by the brown rot fungus Neolentinus lepideus. *Eur. Food Res.* **2020**, *246*, 1773–1782.

[64] Neves, A. C.; Harnedy, P. A.; O'Keeffe, M. B.; FitzGerald, R. J. Bioactive peptides from Atlantic salmon (*Salmo salar*) with angiotensin converting enzyme and dipeptidyl peptidase IV inhibitory, and antioxidant activities. *Food Chem.* **2017**, *218*, 396–405.

[65] Nakamura, T.; Hirota, T.; Mizushima, K.; Ohki, K.; Naito, Y.; Yamamoto, N.; Yoshikawa, T. Milk-derived peptides, Val-Pro-Pro and Ile-Pro-Pro, attenuate atherosclerosis development in apolipoprotein E–deficient mice: a preliminary study. *J. Med. Food* **2013**, *16*, 396–403.

[66] Liao, W.; Fan, H.; Davidge, S. T.; Wu, J. Egg white–derived antihypertensive peptide IRW (Ile-Arg-Trp) reduces blood pressure in spontaneously hypertensive rats via the ACE2/ang (1-7)/mas receptor Axis. *Mol. Nutr. Food Res.* **2019**, *63*, 1900063.

[67] Son, M.; Chan, C. B.; Wu, J. Egg white ovotransferrin-derived ACE inhibitory peptide ameliorates angiotensin II-stimulated insulin resistance in skeletal muscle cells. *Mol. Nutr. Food Res.* **2018**, *62*,

1700602.

[68] Jiao, H.; Zhang, Q.; Lin, Y.; Gao, Y.; Zhang, P. The ovotransferrin-derived peptide IRW attenuates lipopolysaccharide-induced inflammatory responses. *Biomed Res. Int.* **2019**, *2019*.

[69] Kovacs-Nolan, J. M.; Zhang, H.; Ibuki, M.; Nakamori, T.; Yoshiura, K.; Turner, P. V.; Matsui, T.; Mine, Y. The PepT1-transportable soy tripeptide VPY reduces intestinal inflammation. *Biochim. Biophys. Acta. Gen. Subj.* **2012**, *1820*, 1753–1763.

[70] Merz, K. E.; Thurmond, D. C. Role of skeletal muscle in insulin resistance and glucose uptake. *Compr. Physiol.* **2011**, *10*, 785–809.

[71] Wijesekara, N.; Thong, F. S.; Antonescu, C. N.; Klip, A. Diverse signals regulate glucose uptake into skeletal muscle. *Can. J. Diabetes* **2006**, *30*, 80–88.

[72] Qiu, J.; Maekawa, K.; Kitamura, Y.; Miyata, Y.; Tanaka, K.; Tanaka, T.; Soga, M.; Tsuda, T.; Matsui, T. Stimulation of glucose uptake by theasinensins through the AMP-activated protein kinase pathway in rat skeletal muscle cells. *Biochem. Pharmacol.* **2014**, *87*, 344–351.

[73] Liu, L.; Zheng, J.; Zhou, M.; Li, S.; He, G.; Wu, J. Peptide analogues of VPP and IPP with improved glucose uptake activity in L6 myotubes can be released from cereal proteins. *J. Agric. Food Chem.* **2021**, *69*, 2875–2883.

[74] Iwasa, M.; Takezoe, S.; Kitaura, N.; Sutani, T.; Miyazaki, H.; Aoi, W. A milk casein hydrolysate-derived peptide enhances glucose uptake

through the AMP-activated protein kinase signalling pathway in skeletal muscle cells. *Exp. Physiol.* **2021**, *106*, 496–505.

[75] Straub, L. G.; Scherer, P. E. Metabolic messengers: adiponectin. *Nat. Metab.* **2019**, *3*, 334–339.

[76] Choi, S. R.; Lim, J. H.; Kim, M. Y.; Kim, E. N.; Kim, Y.; Choi, B. S.; Park, C. W. Adiponectin receptor agonist AdipoRon decreased ceramide, and lipotoxicity, and ameliorated diabetic nephropathy. *Metab.: Clin. Exp.* **2018**, *85*, 348–360.

[77] Choi, S. K.; Kwon, Y.; Byeon, S.; Haam, C. E.; Lee, Y. H. AdipoRon, adiponectin receptor agonist, improves vascular function in the mesenteric arteries of type 2 diabetic mice. *PLoS One* **2020**, *15*, e0230227.

[78] Zou, C.; Wang, Y.; Shen, Z. 2-NBDG as a fluorescent indicator for direct glucose uptake measurement. *J. Biochem. Biophys. methods* **2005**, *64*, 207–215.

[79] Nishiumi, S.; Ashida, H. Rapid preparation of a plasma membrane fraction from adipocytes and muscle cells: application to detection of translocated glucose transporter 4 on the plasma membrane. *Biosci. Biotechnol. Biochem.* **2007**, *71*, 2343–2346.

[80] Jo, S.; Kim, T.; Iyer, V. G.; Im, W. CHARMM-GUI: a web-based graphical user interface for CHARMM. *J. Comput. Chem.* **2008**, *29*, 1859–1865.

[81] Boonstra, S.; Onck, P. R.; van der Giessen, E. CHARMM TIP3P water

model suppresses peptide folding by solvating the unfolded state. *J. Phys. Chem. B* **2016**, *120*, 3692–3698.

[82] Maier, J. A.; Martinez, C.; Kasavajhala, K.; Wickstrom, L.; Hauser, K. E.; Simmerling, C. ff14SB: improving the accuracy of protein side chain and backbone parameters from ff99SB. *J. Chem. Theory Comput.* **2015**, *11*, 3696–3713.

[83] Dickson, C. J.; Madej, B. D.; Skjevik, Å. A.; Betz, R. M.; Teigen, K.; Gould, I. R.; Walker, R. C. Lipid14: the amber lipid force field. *J. Chem. Theory Comput.* **2014**, *10*, 865–879.

[84] Wang, J.; Wolf, R. M.; Caldwell, J. W.; Kollman, P. A.; Case, D. A. Development and testing of a general amber force field. *J. Comput. Chem.* **2004**, *25*, 1157–1174.

[85] Case, D. A.; Cheatham III, T. E.; Darden, T.; Gohlke, H.; Luo, R.; Merz Jr, K. M.; Onufriev, A.; Simmerling, C.; Wang, B.; Woods, R. J. The Amber biomolecular simulation programs. *J. Comput. Chem.* **2005**, *26*, 1668–1688.

[86] Kollman, P. A.; Massova, I.; Reyes, C.; Kuhn, B.; Huo, S.; Chong, L.; Lee, M.; Lee, T.; Duan, Y.; Wang, W.; Donini, O.; Cieplak, P.; Srinivasan, J.; Case, D. A.; Cheatham, T. E. Calculating structures and free energies of complex molecules: combining molecular mechanics and continuum models. *Acc. Chem. Res.* **2000**, *33*, 889–897.

[87] Miyagusuku-Cruzado, G.; Morishita, N.; Fukui, K.; Terahara, N.; Matsui, T. Anti-prediabetic effect of 6-*O*-caffeoylsophorose in prediabetic rats

and its stimulation of glucose uptake in L6 myotubes. *Food Sci. Technol. Res.* **2017**, *23*, 449–456.

[88] Vlavcheski, F.; Naimi, M.; Murphy, B.; Hudlicky, T.; Tsiani, E. Rosmarinic acid, a rosemary extract polyphenol, increases skeletal muscle cell glucose uptake and activates AMPK. *Molecules* **2017**, *22*, 1669.

[89] Zygmunt, K.; Faubert, B.; MacNeil, J.; Tsiani, E. Naringenin, a citrus flavonoid, increases muscle cell glucose uptake via AMPK. *Biochem. Biophys. Res. Commun.* **2010**, *398*, 178–183.

[90] Rodríguez, Y.; Májeková, M. Structural Changes of Sarco/Endoplasmic Reticulum Ca^{2+}-ATPase Induced by Rutin Arachidonate: A Molecular Dynamics Study. *Biomolecules* **2020**, *10*, 214.

[91] Banerjee, S.; Talukdar, I.; Banerjee, A.; Gupta, A.; Balaji, A.; Aduri, R. Type II diabetes mellitus and obesity: Common links, existing therapeutics and future developments. *J. Biosci.* **2019**, *44*, 1–13.

[92] Patil, P.; Mandal, S.; Tomar, S. K.; Anand, S. Food protein-derived bioactive peptides in management of type 2 diabetes. *Eur. J. Nutr.* **2015**, *54*, 863–880.

[93] C de Campos Zani, S.; Wu, J.; B Chan, C. Egg and soy-derived peptides and hydrolysates: A review of their physiological actions against diabetes and obesity. *Nutrients* **2018**, *10*, 549.

[94] Azadbakht, L.; Atabak, S.; Esmaillzadeh, A. Soy protein intake, cardiorenal indices, and C-reactive protein in type 2 diabetes with

nephropathy: a longitudinal randomized clinical trial. *Diabetes Care* **2008**, *31*, 648–654.

[95] Hansen, P. R.; Oddo, A. Fmoc solid-phase peptide synthesis. *Methods Mol. Biol.* **2015**, *1348*, 33–50.

[96] Hanh, V. T.; Kobayashi, Y.; Maebuchi, M.; Nakamori, T.; Tanaka, M.; Matsui, T. Quantitative mass spectrometric analysis of dipeptides in protein hydrolysate by a TNBS derivatization-aided standard addition method. *Food Chem.* **2016**, *190*, 345–350.

[97] Kumari, R.; Kumar, R. *g_mmpbsa*–A GROMACS tool for high-throughput MM-PBSA calculations. *J. Chem. Inf. Model.* **2014**, *54*, 1951–1962.

[98] Samoto, M.; Maebuchi, M.; Miyazaki, C.; Kugitani, H.; Kohno, M.; Hirotsuka, M.; Kito, M. Abundant proteins associated with lecithin in soy protein isolate. *Food Chem.* **2007**, *102*, 317–322.

[99] Kim, E. D.; Bayaraa, T.; Shin, E. J.; Hyun, C. K. Fibroin-derived peptides stimulate glucose transport in normal and insulin-resistant 3T3-L1 adipocytes. *Biol. Pharm. Bull* **2009**, *32*, 427–433.

Acknowledgements

Throughout my doctoral study, I have received a great deal of support and assistance. First and foremost, I would like to express my profound gratitude to my supervisor, Prof. Toshiro Matsui, for his continuous guidance, encouragement, and support during my Ph.D. study. His professional perspective and insightful feedback pushed me to sharpen my academic thinking and brought my research to a higher level.

Besides my supervisor, I would like to thank Prof. Mitsuhiro Furuse and Assoc. Prof. Mitsuru Tanaka for taking the time to review my dissertation and provide their precious comments. I would like to thank Prof. Noriatsu Shigemura and Dr. Keisuke Sanematsu for their scientific comments and suggestions. I would also like to thank the Research Institute for Information Technology of Kyushu University for providing the research supercomputing services.

I would like to thank Assoc. Prof. Mitsuru Tanaka and Ms. Kaori Miyazaki who have been generous in helping me to live a stable life in Japan. I would like to thank my partner Akihiro Nakano for his scientific support and giving me words of encouragement. Thanks to all my other members in Laboratory of Food Analysis for their kind help.

I would like to thank to ASSURAN International Scholarship Foundation for the financial support during my Ph.D. study.

Most of all, I would like to express my sincere gratitude to my parents and two sisters who always believed and supported me. Without their active supports, I would not have the courage to start my Ph.D. study in Japan.